Photodiagnosis and Photodynamic Therapy 26 (2019) 162–178

Contents lists available at ScienceDirect

Photodiagnosis and Photodynamic Therapy

journal homepage: www.elsevier.com/locate/pdpdt

Role of various nanoparticles in photodynamic therapy and detection methods of singlet oxygen

Jan Krajczewski[a,*], Karolina Rucińska[b], Helen E. Townley[c], Andrzej Kudelski[a]

[a] Faculty of Chemistry, University of Warsaw, ul. Pasteura 1, 02-093 Warsaw, Poland
[b] Medical University of Warsaw, Żwirki i Wigury 61, 02-091 Warsaw, Poland
[c] Nuffield Department of Women's and Reproductive Health, University of Oxford, John Radcliffe Hospital, Oxford, UK Department of Engineering Sciences, University of Oxford, Oxford, UK

ARTICLE INFO

Keywords:
Nanomaterials
Cancer treatment
PDT
Nanomaterials in PDT
Nanoparticles
Nanomedicine
Photodynamic therapy

ABSTRACT

In this review article we described the applications of various nanoparticles that can be used for photodynamic therapy (PDT), such as: plasmonic nanoparticles, quantum dots and upconversion nanoparticles. In comparison with typical organic photosensitizers such as hematoporphyrins, they exhibit higher photostability and resistance to enzymatic degradation, and hence, in some cases, they could replace organic photosensitizers in PDT therapy. It has also been found that the presence of plasmonic noble metal nanoparticles increases the efficiency of conjugated standard photosensitizers. Therefore, one can expect that, due to their very promising optical properties, plasmonic nanoparticles, plasmonic composites, and upconversion nanoconjugates will have a significant impact on the detection and treatment of cancer in the near future. Various methods of detecting the singlet oxygen produced are also reviewed.

1. Introduction

In the 21st century, the main causes of death are various types of cancer and heart disease. Surgery is the primary method of treatment for isolated, solid tumors, and is usually followed by chemo- or radiotherapy. However, the side effects of such adjuvant therapies can be severe, and new, non–invasive methods of treatment are sought. One such option is photodynamic therapy (PDT), in which a photosensitizer is introduced to the organism and the tissue containing abnormal cells is illuminated. The light excites the photosensitizer (usually some kind of organic molecule) and there is a transfer of energy to an oxygen molecule in the ground state and the formation of an excited singlet oxygen molecule. The typical organic photosensitizers currently in use can easily be decomposed by enzymes. Plasmonic metal nanoparticles could in some cases replace organic photosensitizers in PDT therapy. It has also been found that the presence of plasmonic nanoparticles increases the efficiency of conjugated standard photosensitizers. Moreover, some semiconductor nanoparticles with a suitably matched energy gap could be used as photosensitizers, and these nanosystems could be also conjugated with certain standard organic photosensitizers. In such systems, energy is transferred from the excited nanoparticles (e.g. quantum dots) to photosensitizer molecules due to a FRET mechanism. Another group of nanoparticles suitable for photodynamic therapy are upconversion nanoparticles. Due to the light upconversion phenomenon, these nanoparticles can be excited by near-infrared radiation and emit light having a shorter wavelength, which leads to the excitation of the organic photosensitizer. In this review article, we present the roles of various kinds of nanoparticles in PDT. Various methods of detecting the singlet oxygen produced are also reviewed.

2. PDT history

Porphyrins were first tested on humans as early as 1913, when Friedrich Meyer– Betz found that the application of haematoporphyrin to his own skin resulted in pain in areas exposed to light exposed [1]. In the 1950s, a haematoporphyrin derivative HPD (see Fig. 1) that was obtained by treating haematoporphyrins with acetic and sulphuric acids [2] was found to localize to tumours and emit fluorescence [3,4]. Initially, HPD was considered to be a very promising diagnostic tool, but later it was postulated that such porphyrins could exhibit phototoxic properties and might be used to kill cancer cells [5]. *In vivo* tests subsequently carried out showed that porphyrins could delay the growth of gliomas implanted in rats. The tumour growth could be stopped for 10–20 days, although after that time the deeper regions of the tumour began to grow again. Later work reported the possibility of applying HPD in conjunction with irradiation with red light to eradicate mammary tumor growth in

* Corresponding author.
E-mail address: jkrajczewski@chem.uw.edu.pl (J. Krajczewski).

https://doi.org/10.1016/j.pdpdt.2019.03.016
Received 15 December 2018; Received in revised form 18 March 2019; Accepted 22 March 2019
Available online 23 March 2019

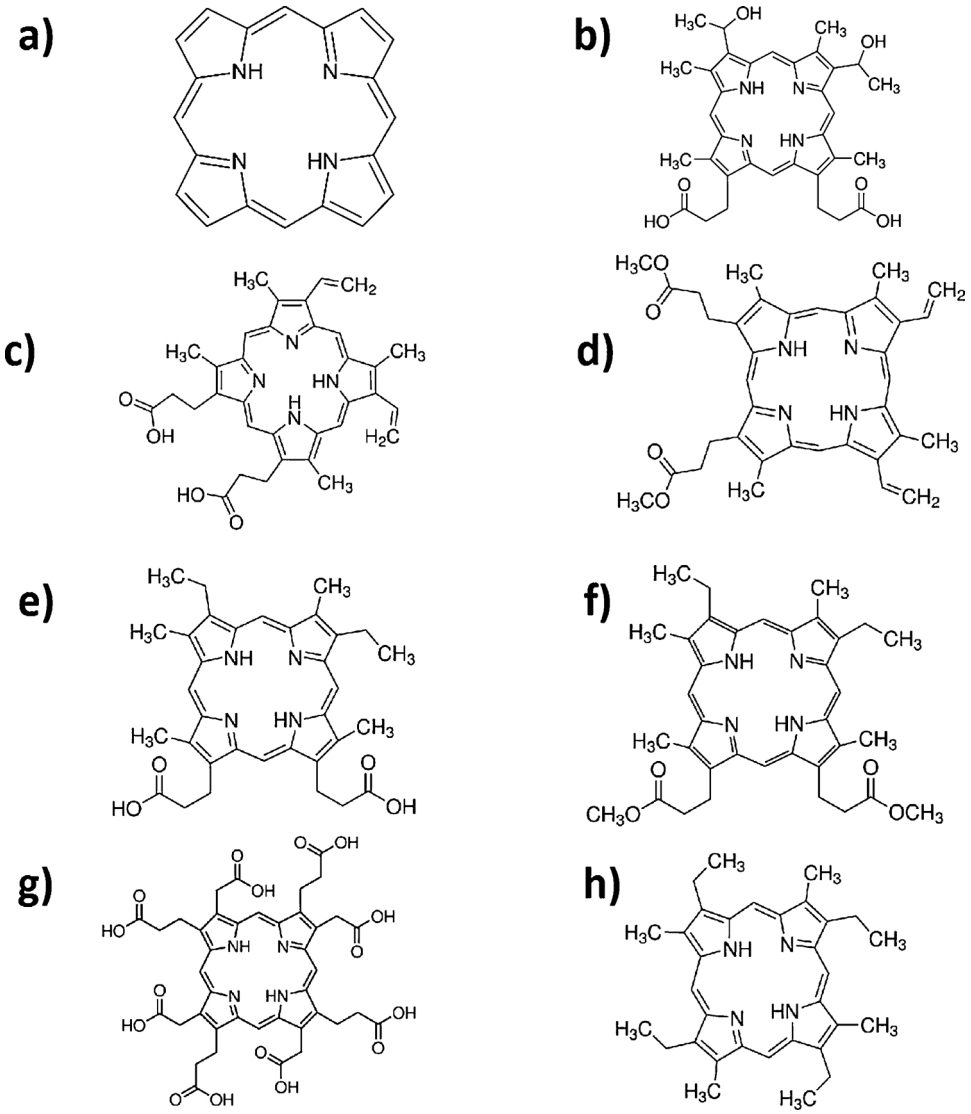

Fig. 1. Structural formulas of porphyrin, hematoporhyrin and hematoporphyrins derivatives (HPD): a) porphyrin, b) hematoporhyrin, c) protoporphyrin IX, d) protoporphyrin IX diethyl ester, e) mesoporphyrin, f) mesoporphyrin diethyl ester, g) uroporphyrin and h) etioporphyrin.

mice [6], and in the same year it was shown that light activated HPD could eliminate bladder carcinoma in mice [7]. This study was subsequently extended to show that light-activated HPD could be used to treat bladder cancer in humans [8]. The tests indicated that there was slower tumor growth and tumor necrosis in those areas which received PDT. Following this initial experiment, other teams applied PDT to treat lung tumours [9,10], gastric carcinomas [11], brain tumors [12–15] head and neck tumours [16,17] and colorectal cancers [18].

In addition to porphyrins, it was reported that common dyes such as methylene blue (MB) [19], Rose Bengal (RB) [20] or eosyin Y [21] could be used as photosensitizers. Methylene blue, for example, exhibits a strong absorption band (85,000 $M^{-1} cm^{-1}$) at 664 nm [22]. The maximum quantum yield of singlet oxygen generation by MB is estimated to be 0.5 [23]. Rose Bengal has an absorption maximum at 559 nm (90,400 $M^{-1} cm^{-1}$), and exhibits an even higher quantum yield of 0.75 [24]. The cost of such dyes is considerably lower than that of porphyrins, and therefore such compounds are also very promising candidates for commercial photosensitizers. All of the above dyes, however, exhibit absorption bands in the visible region, where the penetration of radiation through biological tissues is highly limited. The strongest shift of the absorption band into the infra-red region can be observed in the case of phthalocyanines. Zn naphthalocyanine, for example, exhibits a strong absorption band (160 000 $M^{-1} cm^{-1}$) at 764 nm, with the singlet oxygen quantum yield estimated to be 0.45 [25]. Of course, in addition to the mentioned model systems, many drugs that have been clinically-approved or are undergoing clinical trials are used for PDT (see Table 1). For example, Photofrin® (porfimer sodium) can be injected intravenously and is still widely used for PDT treatment of various cancers such as lung, bladder or cervical cancer [26,27]. However, Photofrin® persists for more than 2 months after administration. In case of head and neck cancer, Foscan® (temoporfin) can be used [28]. There are also some drugs that can be activated with near-infrared radiation, such as: Lutex® (motexafin lutetium) or Tookad® (palladium bacteropheophoride). Lutex® can be activated by radiation in a range between 730 and 770 nm, and Tookad® by radiation with a wavelength of about 760 nm. For prostate cancer in phase II or III, Tookad® is administered as a single dose by intravenous injection 10 min before irradiation. The drug accumulates selectively in tumour blood vessels and has a fast clearance (half-life 0.02 - 0.03 h) [29].

3. Photodynamic processes and detection of singlet oxygen

PDT leads to tumour destruction by the generation during irradiation of highly toxic singlet oxygen. This singlet oxygen can either (I) kill the tumor cell directly, or (II) damage tumor-associated vasculature. Furthermore, PDT (III) can activate an immune response against the

Table 1
Organic photosensitizers for PDT clinically approved or undergoing clinical trials.

Clinically approved			
Generic name	Chemical name	Maximum of absorption [nm]	Application
Foscan	Temoporfin	652	Prostate cancer, head and neck cancer
Visudyne	Verteporfin	690	Pancreatic cancer
Laserphyrin	Talaporfin	664	Head and neck cancer
Photofrin	Porfimer sodium	630	Esophageal cancer, lung cancer and adenocarcinoma
Levulan/Ameluz	Aminolevulinic acid	635	Actinic keratosis
Redaporfin	Redaporfin	749	Biliary tract cancer
Undergoing clinical trials			
TOOKAD	Palladium bacteriopheophorbide	762	Prostate cancer in phase II or III
Lutex	Metaxafin lutetium	730 & 770	Prostate cancer
Xcytrin	Metaxafin gadolinum	742	Brain metastasis, lung cancer
Talaporfin	Aspartyl chlorin	664	Colorectal neoplasms
Metvixia	Methyl aminolevulinate	570 – 670	Actinic keratosis and basal cell carcinoma
Radachlorin	Aspartyl chlorin	662	Skin cancer

tumor, and most likely a combination of all these three factors is required for effective tumor treatment. Therefore, to effectively evaluate novel materials for PDT, it is important to quantify the generation of singlet oxygen.

After the absorption of a photon by a molecule of the photosensitizer, that molecule is transformed from a ground singlet state to a short–lived, excited singlet state. Due to non–radiative transition, it is then possible to change the multiplicities of the photosensitizer from singlet to a long–lived triplet state. The excited photosensitizer in the triplet state can then decay via two different processes (see Fig. 2). It can produce radicals and radical ions in its surroundings (type I), or its energy can be transferred to an oxygen molecule in the ground state which leads to the formation of a singlet excited oxygen molecule (type II). Both processes occur simultaneously, and the ratio between the type I and type II processes depends on the specific photosensitizer used. It is estimated that the average lifetime of an excited oxygen molecule is shorter than 0.04 μs. Therefore, in *in-vivo* conditions, molecules of excited oxygen can only act over a distance of about 0.02 μm from the place where they are synthesised.

As mentioned above, light interacting with a photosensitizer generates singlet oxygen. In the case of *in vivo* or *in vitro* tests, the generation of singlet oxygen can be observed indirectly through the reduction that occurs in the cell survival rate. However, the first tests are usually carried out without using tissues or cell cultures, and so, instead of living cells, some molecules sensitive to singlet oxygen are used for these measurements.

Singlet oxygen $^1O_2$ has an energy level of 94.29 kJ mol^{-1} above the triplet ground state. The amount of energy corresponds to a transition in the near-infrared region at ~1270 nm. Therefore, one method for detecting singlet oxygen involves a direct phosphorescence measurement of the emission at 1270 nm (Fig. 3).

Many other methods of detecting singlet oxygen are based on an analysis of the interaction between molecules of the singlet oxygen and a substance sensitive to this compound (see Table 2). Depending upon the exact nature of the interaction with a sensor molecule, the change in its structure can be monitored by different spectroscopic techniques such as: NMR, EPR, UV–vis absorption, or fluorescence. One example of a sensor compound is 9,10-diphenylanthracene (DPA). In the presence of singlet oxygen, a decrease in the intensity of its absorption band at 355 nm is observed, which decrease is proportional to the amount of

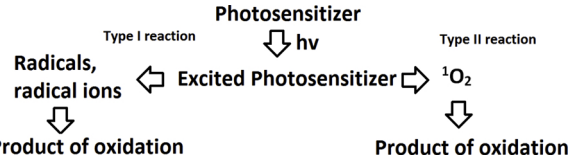

Fig. 2. Scheme presenting two types of process after excitation of the photosensitizer.

the singlet oxygen generated in the system [29]. However, the main disadvantage of DPA as a sensor for singlet oxygen is its poor solubility in water (although it is soluble in many organic solvents such as benzene, toluene, or DMSO). A number of DPA derivatives have been synthesized mainly with the aim of improving its poor solubility. One of the most commonly used derivatives of DPA is 9,10-anthracenediyl-bis (methylene)dimalonic acid (ABDA), which reacts irreversibly with singlet oxygen. The progress of this reaction can be monitored by a decreasing in the intensity of the ABDA absorption band around 382 nm (see Fig. 4). Another derivative, 9,10-anthracenedipropionic acid (ADPA), shows a decrease in the intensity of the absorption peak at 400 nm upon reaction with singlet oxygen. Other DPA derivatives applied for the detection of singlet oxygen include anthracene-9,10-diyl-diethyl disulfate (EAS), anthracene-9,10-bisethanesulfonic acid (AES), anthracene-9,10-divinylsulfonate (AVS), bis-9,10-anthracene-(4-trimethyl-phenylammonium)dichloride (BPAA), N,N0-di-(2,3-dihydroxypropyl)-9,10-anthracene- dipropanamide (DHPA), and sodium 1,3-cyclohexadiene-1,4-diethanoate (CHDDE) [30–37].

Another widely used compound for spectrophotometrical detection of singlet oxygen is 1,3-diphenylisobenzofuran (DPBF). In the presence of singlet oxygen, DPBF immediately forms an unstable endoperoxide which decomposes to 1,2-dibenzoylbenzene. DPBF exhibits a strong absorption band at 415 nm, and the decrease in absorption at this wavelength is proportional to the amount of the singlet oxygen formed.

Fluorescence measurements may be also used when the interaction of singlet oxygen with a fluorescence probe leads to changes in the fluorescence intensity, wavelength, quantum yield, or fluorescence lifetime. Historically, the first fluorescence probe used for the detection of singlet oxygen was 9-[2-(3-carboxy-9,10-diphenyl)anthryl]-6-hydroxy-3H-xanthen-3-one (DPAX). DPAX is not fluorescent until it interacts with singlet oxygen and forms the endoperoxide (DPAX-EPs), which is strongly fluorescent and has a high quantum yield [38]. However, DPAX cannot be used in acidic environments. A similar molecule, 9-[2-(3-carboxy-9,10-dimethyl)anthryl]-6-hydroxy-3H-xanthen-3-one (DMAX), is also only fluorescent in its endoperoxide form, but is much more sensitive and less hydrophobic, and therefore can be applied for biological samples [39].

In recent years, the most commonly used fluorescence probe has been the Singlet Oxygen Sensor Green (SOSG), commercialized by Invitrogen/Molecular Probes. This indicator initially exhibits weak blue fluorescence, but in the presence of singlet oxygen emits a green fluorescence when excited at 504 nm [40]. SOSG is highly selective for singlet oxygen, and does not show any appreciable response to hydroxyl or superoxide radicals. SOSG is intended for use in an aqueous environment. Due to the high quantum yield of SOSG fluorescence, the suggested starting concentration of SOSG can be very low (usually in a range between 1 and 10 μM).

Some rare earth chelate complexes can be also used to detect singlet oxygen. In comparison with organic fluorescence probes, these

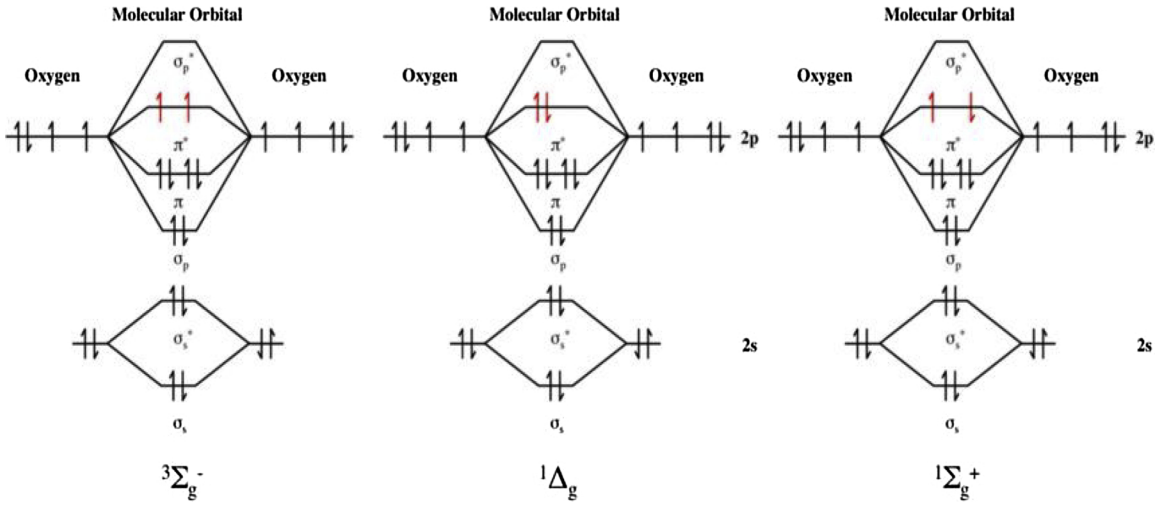

Fig. 3. Molecular orbital diagram of triplet ground state ($^3\Sigma_g^-$) and two singlet excited states ($^1\Delta_g$) and ($^1\Sigma_g^+$) of molecular dioxygen.

Table 2
Detection methods of singlet oxygen.

Property	Sensor molecule		Changes caused by singlet oxygen
Light absorption	9,10-diphenylanthracene	DPA	Decrease peak at 355 nm
Light absorption	9,10-anthracenediyl-bis(methylene)dimalonic acid	ABDA	Decrease peak at 382 nm
Light absorption	9,10-anthracenedipropionic acid	ADPA	Decrease peak at 400 nm
Light absorption	anthracene-9,10-bisethanesulfonic acid	AES	Decrease peaks at 360, 378 and 400 nm
Light absorption	1,3-diphenylisobenzofuran	DPBF	Decrease peak at 415 nm
Phosporescence	singlet oxygen		Phosporescence at 1067 nm
Fluorescence	9-[2-(3-carboxy-9,10-diphenyl)anthryl]-6-hydroxy-	DPAX	Fluorescent endoperoxide formation
Fluorescence	3H-xanthen-3-one	DMAX	Fluorescent endoperoxide formation
Fluorescence	9-[2-(3-carboxy-9,10-dimethyl) anthryl]-6-hydroxy-3H-xanthen-3-one	DPBF	Decrease in fluorescence intensity
	1,3-diphenylisobenzofuran		
Fluorescence	Singlet Oxygen Sensor Green	SOSG	Strong green fluorescence
Chemiluminescence	2-methyl-6-phenyl- 3,7-dihydroimidazo [1,2-a] pyrazin-3-one	CLA	Strong chemiluminescence
NMR	Cyclohexene		Change in NMR spectrum
EPR	2,2,6,6-tetramethylpiperidine	TEMP	Change in EPR spectrum

compounds exhibit larger Stokes shifts and sharper emission curves when used for this purpose. The most commonly used rare earths probes are europium and terbium (Eu^{3+}, Tb^{3+}) complexes. A very efficient rare earth complex used for detection of singlet oxygen is [40-(10-methyl-9-anthryl)-2,20 : 60,200-terpyridine-6,600-diyl]bis(methylenenitrilo)tetrakis(acetate)-Eu^{3+}] (MTTA-Eu^{3+}), which has a reported limit of detection of singlet oxygen equal to 3.8 nmol/dm^3 [41]. However, another probe with a lower limit of detection (10.8 nmol/dm^3), *N,N,*N0,N0-[2,6-bis-(30-aminomethyl-10-pyrazolyl)-4-(900-anthryl) pyridine]tetrakis(acetate)-Tb^{3+} (PATA-Tb^{3+}), exhibits improved physicochemical properties such as higher water solubility, a wider pH applicable range, and a longer fluorescence lifetime [42].

The main disadvantage of rare earth probes is that they need UV light excitation, which can damage delicate biological systems. It is possible to red-shift the wavelength of the excitation light of the singlet oxygen probes using rhenium complexes (for example: $Re(CO)_3Cl$(2-(anthracen-9-yl)-1-ethyl-imidazophenanthroline)) instead of complexes of rare earth elements [43]. In the native state mentioned above, rhenium complex does not exhibit fluorescence; however, in the presence of singlet oxygen it becomes highly fluorescent after excitation at 410 nm.

Chemiluminescent probes may be also used to detect singlet oxygen; these probes do not require irradiation and emit light spontaneously in the presence of singlet oxygen. Examples of commonly used chemiluminescent probes are 2-methyl-6-phenyl-3,7-dihydroimidazo[1,2-a] pyrazin-3-one (CLA), and its derivatives MCLA and FLCA [44]. All of these compounds emit light spontaneously in the presence of singlet oxygen. However, they also react with superoxide anion, so their utility is limited.

The $^1\Delta_g$ state of singlet oxygen is paramagnetic, and can be detected in the gas phase using EPR spectroscopy [45]. The recorded spectrum of singlet oxygen is an almost symmetrical quartet. It is well known that cyclohexene is able to react with singlet oxygen. The major product of this reaction is 2-hydroperoxyl cyclohexene. The formation of 2-hydroperoxyl cyclohexene can be monitored, for example, by NMR spectroscopy. [46]. Another useful technique for detecting singlet oxygen is EPR spectroscopy [47], in which case 2,2,6,6-tetramethylpiperidine – TEMP can be used as a sensor molecule. TEMP is nonparamagnetic, however; after interaction with singlet oxygen it is transformed into the paramagnetic adduct 2,2,6,6-tetramethylpiperidine-n-oxyl radical – TEMPO. The EPR spectrum of TEMPO consists of three equally intense lines. The intensity of these spectral lines is proportional to the amount of the singlet oxygen generated.

4. Application of nanoparticles in PDT

4.1. Noble metal plasmonic nanoparticles

Noble metal plasmonic nanoparticles exhibit many advantages over organic photosensitizers. Nanoparticles are much more stable under irradiation than organic dyes (organic dyes can decompose under intense irradiation, which leads to reduced reaction rates). Moreover, gold and silver nanoparticles exhibit significantly higher extinction coefficients than standard organic photosensitizers do.

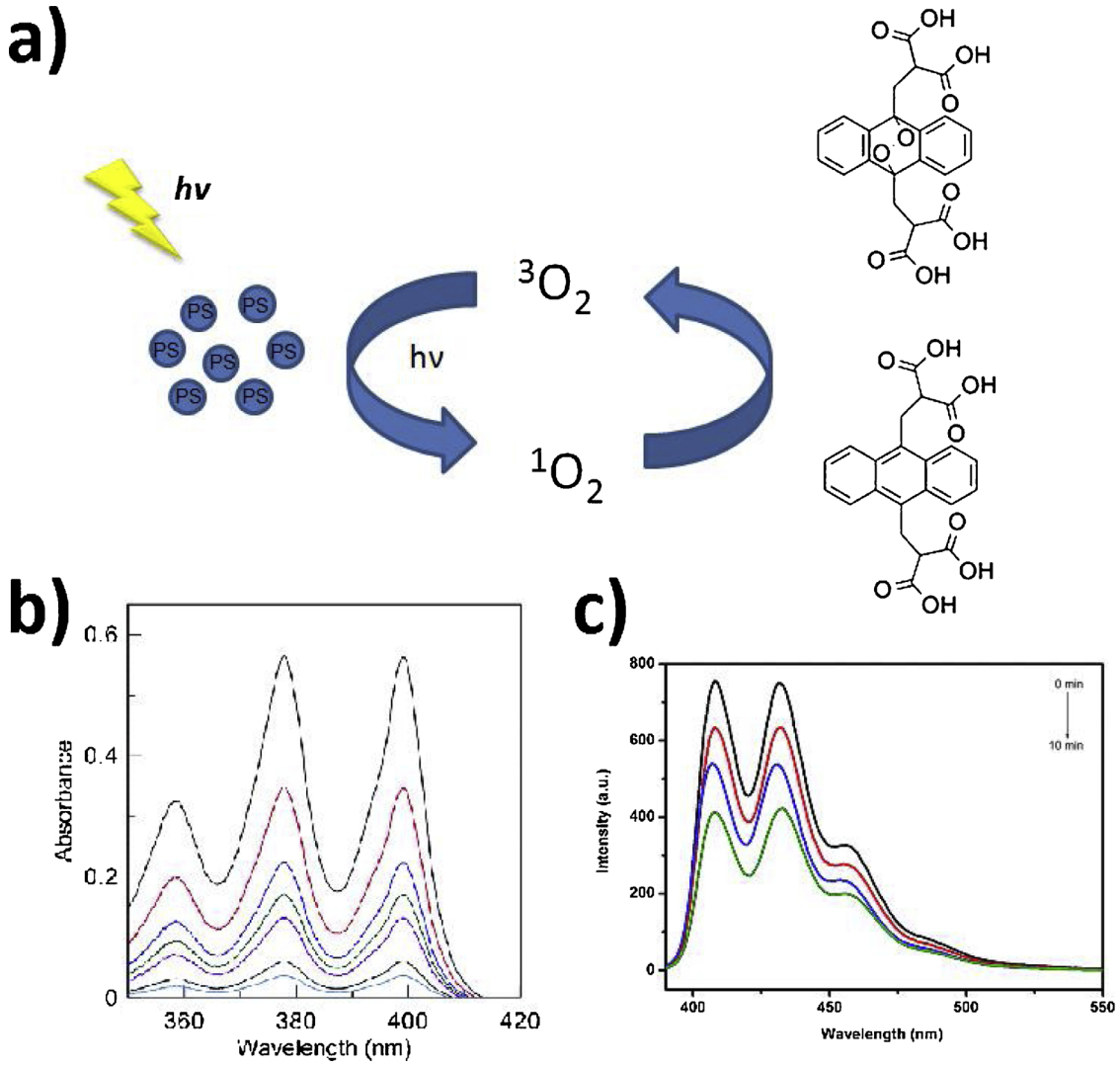

Fig. 4. Scheme illustrating the method of singlet oxygen detection with ABDA molecule as sensor.

As a comparison, Photofrin is one of the most commonly used organic photosensitizers. There are several limitations to this compound. The maximum absorption of Photofrin is at 630 nm. This spectral region is below the biological transparency window. Furthermore, Photofrin does not exhibit high selectivity for tumor tissue, has a complicated structure, and is relatively difficult to synthesize, which means it is expensive. Noble metal nanoparticles are also stable - in contrast to organic photosensitizers, which are known to easily undergo enzymatic degradation.

The human body exhibits a biological transparency window from 650 to 1350 nm. In the case of noble metal nanoparticles, it is possible to control the position of the localised surface plasmon resonance (LSPR) band by varying the size and shape of the nanoparticles; for example, with gold nanorods, by changing the aspect ratio one can shift the position of the LSPR band by over 950 nm.

In order to have an efficient energy transfer from the LSPR in noble metal nanoparticles to the molecular oxygen, thus forming singlet oxygen, some O_2 molecules must be adsorbed on the surface of the plasmonic nanoparticles. Some studies based on low-energy electron diffraction (LEED) measurements have shown that molecular oxygen can be adsorbed on the surfaces of metal crystals [47]. Therefore, a rapid energy transfer from the LSPR in the nanoparticles to O_2 is possible. It has been shown that low-energy surface states of metal nanoparticles can transfer energy to molecular oxygen with a high efficiency and selectivity of the formation of singlet oxygen, whereas the high-energy surface states of nanoparticles transfer the energy of the LSPR to the molecular oxygen with low efficiencies (Figs. 5–11)[42]. Noble metal nanoparticles similar to azulene and their derivatives do not follow Kasha's rule [48], and their excited state behaviour is strongly dependent on the excitation wavelengths.

The first use of gold nanorods in PDT was demonstrated in 2014 [49]. It was shown that gold nanorods excited by NIR radiation (915 nm, 130 mW/cm^2) could generate singlet oxygen and could destroy B16F0 melanoma tumors in mice without the addition of an organic photosensitizer. Moreover, in addition to generating singlet oxygen, the irradiation of gold nanoparticles induced a strong local temperature increase, which is the basis of photothermal therapy (PTT). Despite the thermal effect, further research proved that PDT is usually much more effective in the destruction of tumors than PTT is. It was observed that PTT treatment using gold nanorods can only suppress the growth of a tumor for a short time, whereas PDT using gold nanorods could completely destroy solid tumours, even when low light doses were used. An analysis of tissue dissected from other organs, such as the liver or spleen, did not show any noticeable off-target damage after PDT. It was estimated that PDT using gold nanorods is at least 10 times more effective than conventional anticancer drugs such as doxorubicin. Furthermore, very low doses of light make it is possible to use an LED array instead of high-power lasers. Gold nanorods have also been

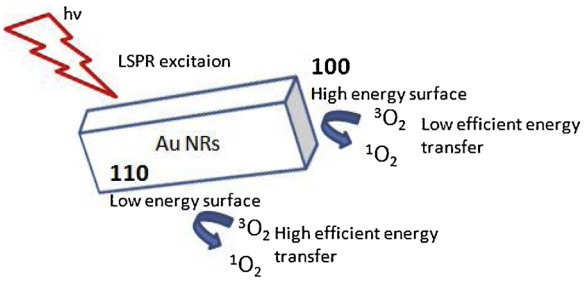

Fig. 5. General scheme showing energy transfer from LSPR in noble metal nanoparticle to molecular oxygen adsorbed.

compared with the organic photosensitizer Rose Bengal (RB) - ABDA has been used to monitor the singlet oxygen generation [50]. It was observed that after irradiation using a continuous-wave diode laser generating radiation with a wavelength of 532 nm, the efficiency of PDT therapy with gold nanorods was significantly lower than in the case of RB. In contrast, under excitation using a femtosecond laser working at 808 nm, the efficiency of the singlet oxygen generation was higher than in the case of RB illuminated at 532 nm. Gold nanorods were also used to test cellular cytotoxicity *in vitro* against HeLa cells. The cell viability without any photosensitizer remained at almost 100% after 15 min of laser irradiation, demonstrating that the laser irradiation power used was safe for cells and do not lead to any detectable damage. However, the cell viability incubated with gold nanorods decreased significantly with an increase in illumination time. For example, in the case of gold nanorods with SPR at 808 nm, after 15 min of exposure to 808 nm laser pulses, cell viability decreased to 18%. Hela cells treated with RB under the same conditions displayed only an insignificant killing effect.

Gold nanoechinus structures showed exceptionally high extinction coefficients (~10^{12} M^{-1} cm^{-1}) in the NIR region (800–1700 nm) [51]. During illumination of gold nanoechinus structures with 940 nm radiation, singlet oxygen was detected using SOSG, and the fluorescence signal was more intense when the structures were irradiated with 940 nm light than with 540 nm radiation. It was also shown that the cellular death caused by the phototoxicity of nanoechinus gold nanostructures was much higher for cancerous HeLa cells that for non-cancerous NIH-3T3 fibroblast cells. These differences arise from the different abilities of the cells to withstand oxidative stress. Due to the exceptionally high excitation factor of these gold nanoparticles, the laser powers adopted in this study were 2–3 times lower than the standards set by the American National Standards Institute (ANSI) for skin burning (808 nm @ 330 mW/cm^2, 915 nm @ 340 mW/cm^2, 1064 nm @ 420 mW/cm^2, with exposure times from 10 to 1000 s). In the gold nanoechinus studies, the laser power was 130 mW/cm^2 for all laser wavelengths (880, 915, and 1064 nm).

While the above experiments were performed with continuous-wave lasers, it has been demonstrated that 40 nm spherical gold nanoparticles with an LSPR peak at 524 nm showed greater singlet oxygen generation when pulsed laser light was used [52]. This could lead to an increased yield of PDT for noble metal nanoparticles.

Using gold bipyramids, Ly et al. showed that the maximum efficiency in the generation of singlet oxygen is achieved when the laser wavelength used overlaps with the LSPR peak [53]. Moreover, it was observed that, when excited with the 820 nm radiation, the gold bipyramids with an LSPR peak located at 820 nm generate singlet oxygen more effectively than methylene blue.

Aggregates of gold nanoparticles have been also assessed as photosensitizers for PDT [54]. An aggregation of gold nanoparticles, and hence plasmonic coupling, has been achieved by the addition of cysteine during synthesis. Cysteine is an amino acid containing a thiol group (-SH) that can easily be attached to metallic surfaces *via* the S – Au bond. In acidic environments, cysteine is zwitterionic and can therefore be connected to the surface of other nanoparticles *via* electrostatic interactions, leading to the coupling of gold nanoparticles. After irradiation with a femtosecond 800 nm laser beam (average beam area 0.3 cm^2, 3 W/cm^2, 60 fs pulse, 1 kHz frequency), it was observed that singlet oxygen is generated for both unaggregated and aggregated gold nanoparticles, but the concentration of singlet oxygen was 8.3 times higher for the aggregated spherical nanoparticles than for the isolated ones. A similar effect was observed in the case of aggregated nanorods, where the formation of singlet oxygen was 1.8 times more efficient than in the case of unaggregated gold nanorods. In general, the aggregation of gold nanoparticles usually significantly increased the efficiency of the generation of singlet oxygen.

In addition to unmodified gold spheres and rods, gold nanocages, spherical hollow gold nanoparticles and gold nanorods in shell have also been tested as materials for the generation of singlet oxygen [55]. It has been shown that the molar extinction coefficients at 808 nm increase in the following order: spherical hollow nanoparticles, nanorods in shell, gold nanorods, and gold nanocages. Hollow gold nanoparticles exhibit a strong LSPR peak at about 1100 nm, which is in the body transparency window. It was found that, by varying the shell thickness and particle size, it is possible to tune the plasmon absorption band [56]. By increasing particle size at a constant wall thickness, the absorption band becomes red-shifted. On the other hand, increasing the wall thickness at a constant particle size results in a blue-shift of the

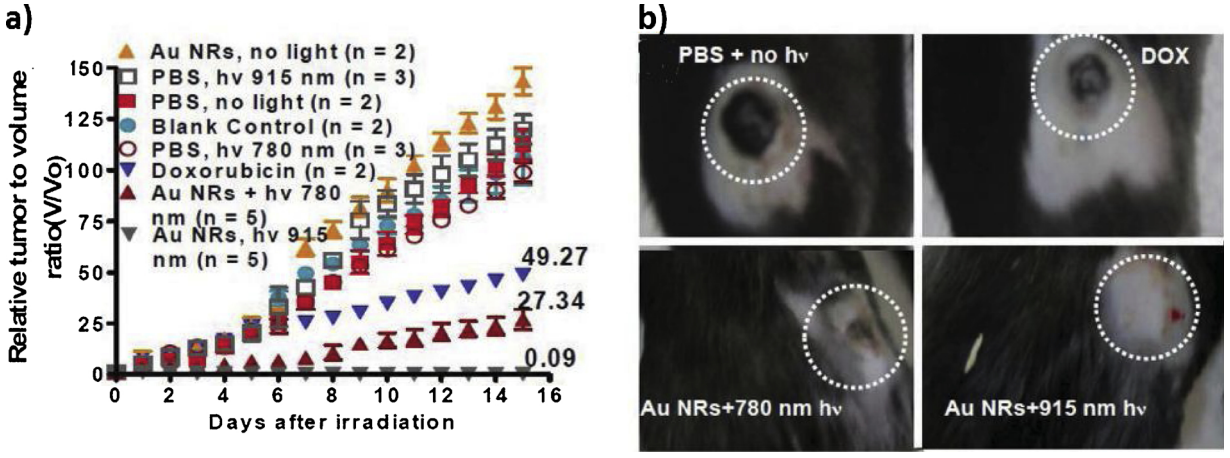

Fig. 6. Results of in vivo photo therapy treatments based on gold nanorods of B16F0 melanoma tumor implanted in mice. a) diagram of tumor volume as a function of time under various conditions (various photosensitizers and wavelength of light); b) images of mice showing tumor size after 14th day after treatment under different conditions. Reprinted with permission from ref. [49]. Copyright 2013 John Wiley and Sons.

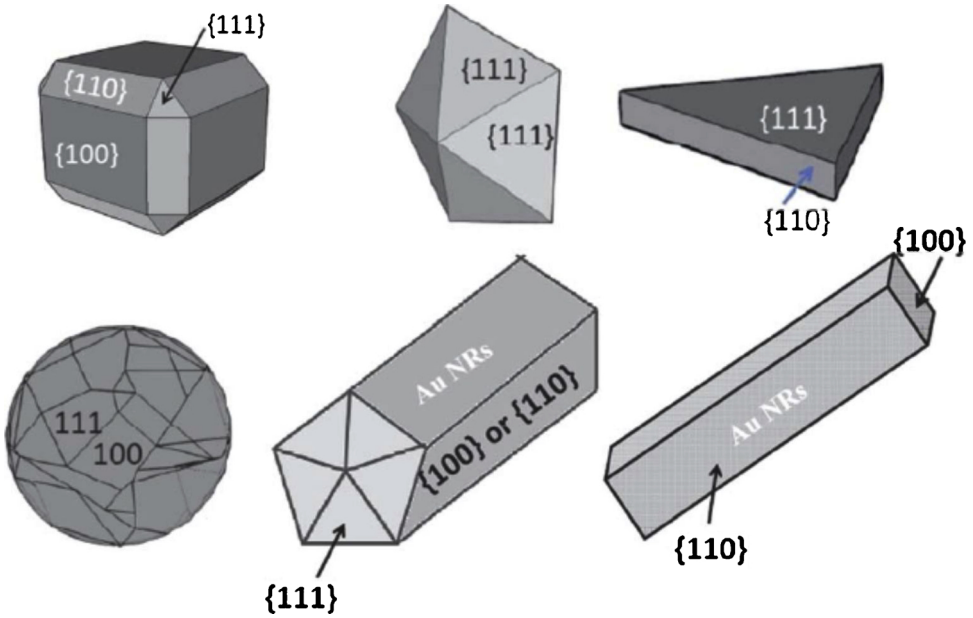

Fig. 7. Correlation of available crystalline surfaces and shapes of nanoparticles. Reprinted with permision from ref. [45]. Copyright 2013 Royal Society of Chemistry.

absorption band. The simple explanation of this phenomenon is that, as the inner diameter of the hollow gold nanoparticles decreases, it takes on, to a higher degree, the properties of solid particles, which exhibit an LSPR peak at 520 nm. Moreover, the absorption cross section of the hollow nanoparticles formed strongly depends on the thickness of the gold shell - as the shell becomes thicker, the absorption cross section becomes larger [57]. Hollow gold nanoparticles effectively generate singlet oxygen during NIR light irradiation (850–1000 nm), but not when visible light is used. When used in *in vitro* experiments against HeLa cells, a significant amount of cell death was observed after irradiation. However, the percentage cell viability was almost 3.4 times lower in the case of irradiation with 940 nm (54 mW/cm^2) light compared to 540 nm (28 mW/cm^2) light. This decrease in efficacy was due to the small amount of singlet oxygen formed upon irradiation at 540 nm. In order to confirm that cellular death was caused by singlet oxygen, the well-known ROS quencher, sodium azide, was added to the samples. Sodium azide significantly increased the viability of the HeLa cells during irradiation by 940 nm light, but there was no change in the case of 550 nm irradiation. This confirmed that cell death after NIR irradiation was connected with the presence of singlet oxygen, while in the case of 550 nm, the smaller amount of cell death was caused by a photothermal effect. The efficacy of the gold nanocage particles was also investigated in mice, in the destruction of B16F0 melanoma tumors during irradiation with 808 nm (150 mW/cm^2 by 13 min) and 980 nm (150 mW/cm^2 by 10 min) laser light. The results obtained showed a significant decrease in the size of the tumours in mice for both wavelengths of light used. Of particular note, the laser powers used were almost 3 times lower than the standard of the American National Standards Institute for skin burning (808 nm = 330 mW/cm^2; 980 nm = 360 mW/cm^2) with exposure time 10–1000 s.

The properties related to the generation of singlet oxygen by gold and silver nanoparticles have been shown to depend on their morphology [45]. It has been observed that irradiating silver decahedron and silver nanoprisms with 885 nm laser light leads to the formation of singlet oxygen, whereas no singlet oxygen was detected when silver nanocubes were used. A similar phenomenon was observed for gold nanoparticles.

The wavelength of the radiation used may not overlap with the LSPR band of the nanoparticles. For example, irradiating silver decahedrons (LSPR band at ca. 520 nm) with NIR 885 nm laser light results in a very strong singlet oxygen phosphorescence signal, whereas irradiating gold decahedrons (having a strong plasmonic band in this wavenumber region) under the same conditions does not result in the formation of singlet oxygen. Similarly, irradiating silver nanoprisms (LSPR band at ca. 590 nm) with 544 nm laser light results in the formation of singlet oxygen, while irradiating silver nanocubes (LSPR

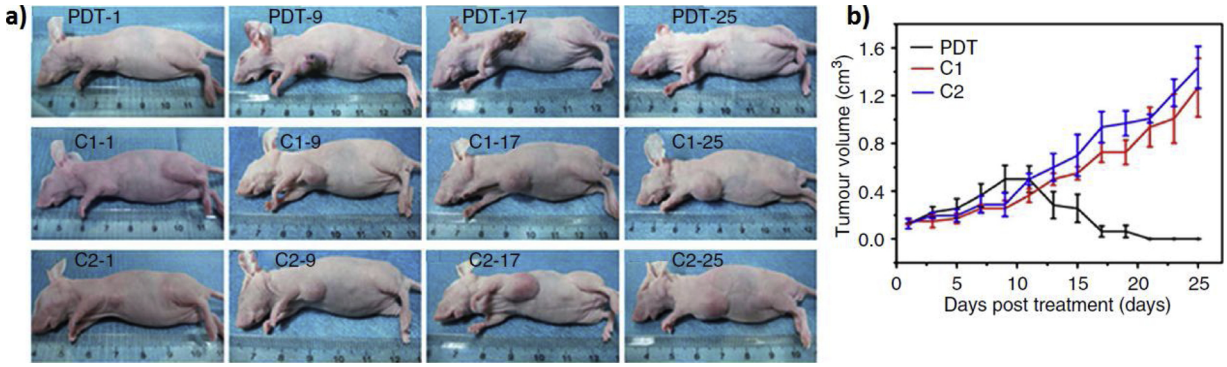

Fig. 8. Results of in vivo photo therapy treatments based on graphene quantum dot of MDA-MB-231 breast tumor implanted mice. a) Photographs of mice after various treatments on the 1 st, 9th, 17th and 25th days. (PDT: GQDs + light irradiation; C1: GQDs only; C2: light irradiation only.); b) Time-dependent tumour growth curves after different treatments. Reprinted with permission from ref. [76]. Copyright 2014 Springer Nature Group.

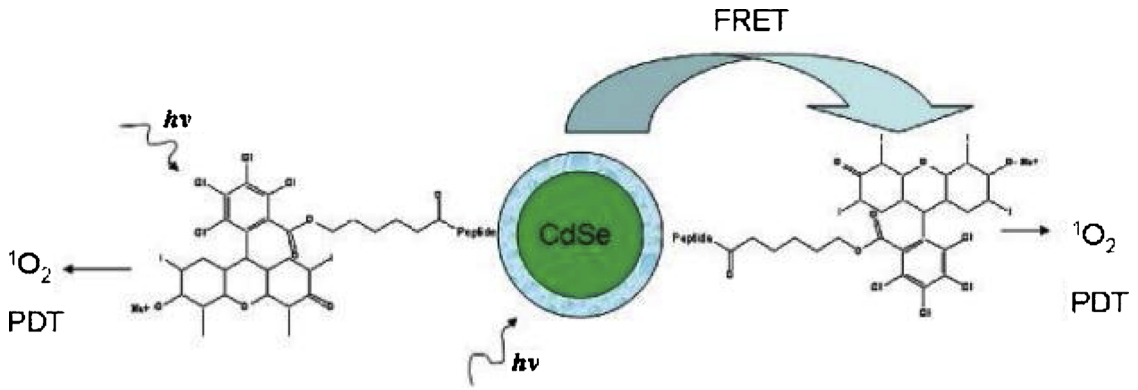

Fig. 9. Proposed mechanisms for singlet oxygen generation based on CdSe/CdS/Zns quantum dots conjugates with RB. Reprinted with permission from ref. [81]. Copyright 2007 American Chemical Society.

band at ca. 500 nm) with 525 nm laser light leads to a weak generation of singlet oxygen, even though the LSPR band of these nanoparticles and the laser light overlap. This implies that the generation of singlet oxygen in the presence of plasmonic noble metal nanoparticles strongly depends on their morphology. Theoretical calculations predict that molecular oxygen could be adsorbed on Au(111), Au(110) and Au(100) surfaces. However, in the case of Au(111) and Au(100) surfaces, oxygen mostly exists in the atomic form. Only in the case of Au(110) crystalline face did the molecular oxygen not dissociate and could it be excited during irradiation to singlet oxygen. In the case of silver nanoparticles, calculations and the experimental techniques have shown that molecular oxygen can be adsorbed on Ag(100), Ag(110) and Ag(111) surfaces. However, in the case of Ag(100) and Ag(110), the surfaces of an adsorbed oxygen molecule will dissociate into atomic form. Therefore, singlet oxygen can only be photosensitized from the Ag(111) crystalline faces, but not on the Ag(100) and Ag(110) crystalline faces. The above relationship may not work perfectly in some cases, due to defects in the shapes of the nanoparticles. Distorted nanocubes, for example, may contain small amounts of 110 or 111 faces where singlet oxygen might possibly be photosensitized. The key factors which permit the application of noble metal nanoparticles in PDT are its morphology and the selective molecular binding of the oxygen molecule to the different crystallographic faces. In the case of silver nanoparticles, singlet oxygen can only be formed on Ag(111) surfaces. Therefore, singlet oxygen can be formed using silver decahedrons or nanoprisms, but not silver nanocubes. Gold nanoparticles were only able to generate singlet oxygen from Au(110) surfaces. Therefore, gold nanorods or bipyramids could be applied to PDT, whereas gold decahedrons cannot generate singlet oxygen.

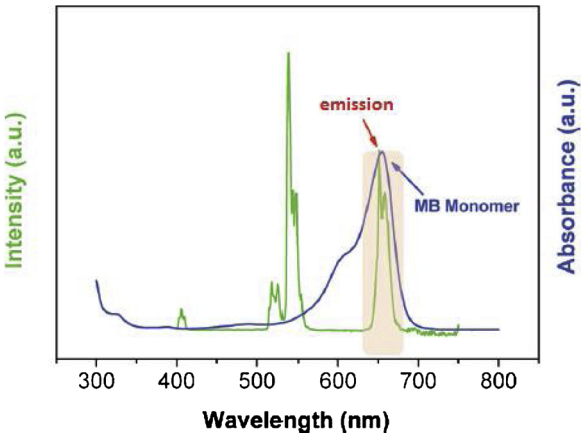

Fig. 11. Absorption spectrum of methylene blue monomer and emission spectrum of NaYF4:Er/Yb/Gd upconversion nanoparticles under excitation using by 980 nm laser light. As mentioned above, the smaller mismatch between the absorption band of the photosensitizer and the emission band of the upconversion nanoparticles leads to a higher efficiency of the process. In the described case, that mismatch is less than 5 nm. Reprinted with permission from ref. [79]. Copyright 2012 John Wiley and Sons.

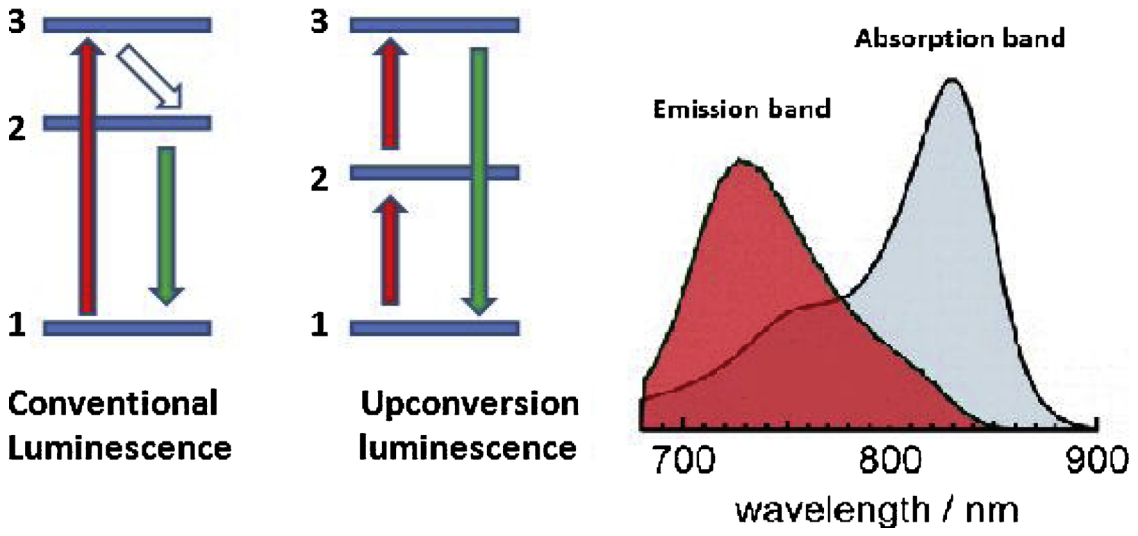

Fig. 10. Schematic presentation of the difference between conventional and upconversion luminescence. The graph presents the localization of the absorption and emission bands in the case of upconversion nanomaterial.

Gold clusters have also been used for PDT. The $Au_{25}(SR)_{18}^-$ cluster (where SR is a general symbol for molecules having a thiol group) can be either water- or organic-soluble, depending on the exact chemical character of the SR part of the cluster [58]. Modifying to form an $Au_{25}(PET)_{18}^-$ cluster resulted in solubility only in organic liquids, which limits its potential in clinical PDT. However, it was observed that $Au_{25}(Capt)_{18}^-$ clusters generated significantly more singlet oxygen than the organic compound methylene blue (irradiation at 650 nm (13 mW/cm^2) and 808 nm (41 mW/cm^2)). To confirm high biocompatibility and efficient singlet oxygen generation, an $Au_{25}(Capt)_{18}^-$ cluster was tested in HeLa cancer cells. The results showed that the viability of the HeLa cells incubated with the $Au_{25}(Capt)_{18}^-$ cluster was drastically reduced after irradiation by 808 nm laser radiation. Cell death could have proceeded via two possible mechanisms: a photothermal or photocytotoxic effect by singlet oxygen. To determine the mechanism, a singlet oxygen scavenger, histidine, was added to the sample. It was observed that cell viability was significantly increased in the presence of histidine, which indicates that in most cases the cancer cells were damaged or killed after interacting with singlet oxygen molecules.

4.2. Plasmonic noble metal nanocomposite

While it has been shown that metal nanoparticles can be effectively used for PDT, the co-incorporation of an organic sensitizer could enhance the properties of the particles. Gold nanostars were prepared and coated with a silica layer to encapsulate the organic photosenzitizer methylene blue in a shell around the nanoparticle [59]. Fluorescence of SOSG was observed even in the case of irradiation by 633 nm laser light at an extremely low power (8 mW). It was observed that these particles produced significantly more singlet oxygen than control silica-coated gold nanostars without embedded MB. It should be noted that no photothermal effects were observed, due to the relatively low laser power (700 mW/cm^2) and excitation with 633 nm light, which did not overlap with the LSPR band of the gold nanostars (800 nm). It was further demonstrated that the MB-loaded nanostars exhibited a cytotoxic effect on BT549 breast cancer cells.

Gold has also been used in conjunction with 5-aminolevulinic acid (5-ALA); a precursor of photoporphyrin IX, which is widely used as a photosensitizer in clinical applications [60,61]. 5-ALA possesses many useful properties, such as low toxicity (before excitation), rapid excretion from the body, and rapid conversion to porphyrins. The main disadvantage of 5-ALA is its zwitterionic character, which significantly limits tissue penetration. In this study, 5-ALA molecules were conjugated to the surface of gold nanoparticles such that the nanoparticles could be used as a transporter. At physiological pH, 5-ALA is negatively charged and can bind to the positively-charged gold surface by electrostatic interaction. The particles were tested against fibrosarcoma cells, where a significant increase in singlet oxygen was observed. Irradiation was carried out using a broadband 150 W halogen lamp for 1 min, and approximately 50% more cancer cells were killed using 5-ALA conjugated to gold nanoparticles than in the standard application of 5-ALA molecules alone. Even more significant is the fact that, in a co-culture system with fibrosarcoma cells, normal fibroblast cells only suffered a minimal effect from the singlet oxygen.

The proporphyrin IX (PpIX) molecule has been also used to functionalize $Ag@SiO_2$ core-shell nanoparticles [42]. The highest efficiency of oxygen generation was gained with 100 nm spherical silver nanoparticles with a 6 nm-thick silica layer containing the PpIX. The amount of singlet oxygen formed was approximately 1.2 and 3.7 times higher than for the free PpIX molecules and silica nanoparticles functionalized with PpIX, respectively. Further increases in the thickness of the silica layer reduced the activity to levels even lower than for the free PpIX solutions. The authors attributed the increased efficiency in the generation of singlet oxygen to the strong electromagnetic force generated by the silver nanoparticles during irradiation. Increasing the distance between the surface of the silver and the PpIX molecules reduces the effective electromagnetic field acting on the photosensitizer molecule and causes a decrease in the yield of the reaction. The authors also underline the importance of the overlap between the absorption band of PpIX and the SPR band of $Ag@SiO_2$ nanoparticles. Gold nanoparticles could also be conjugated with porphyrin derivatives - meso-tetrakis(4-sulphonatophenyl)porphyrin (TPPS) [62].

The shape of the nanoparticles forming the nanocomposite play a critical role in its efficiency in PDT. It has been shown that gold nanorings are 1.43 times more efficient than semi-spherical gold nanoparticles under the same conditions [63]. This is caused by a red-shift of the LSPR band in the case of the gold nanorings. It is assumed that, when the laser light is in resonance with the LSPR of the Au NRs, a substantial enhancement of the EM field occurs in the ring cavity as well as the inner and outer surfaces, which cannot be seen with solid Au NPs.

Gold nanoparticles have also been investigated after being conjugated with the organic photosensitizer phthalocyanine [64]. Phthalocyanine and its zinc derivatives have been successfully used in photodynamic treatment, although the hydrophobic character of phthalocyanine impedes its delivery. It has been shown that gold nanoparticles with an average diameter of 2–4 nm can be functionalized to deliver an organic photosensitizer into tumour cells. When the photosensitizer was bound to the gold surface, the quantum yield of singlet oxygen generation was 0.65, compared with 0.45 for the free photosensiziter. The gold nanoparticles conjugated with phthalocyanine were shown to be effective against HeLa cells, where significant cell mortality through PDT was observed. Furthermore, the conjugation of the photosensitizer to the nanoparticle increases selectivity and biodistribution. A similar approach was presented by P. Calavia *et al.* [65]. However, it was observed that the addition of lactose to the gold nanoaprticle surface selectively targeted the SK-BR-3 cells, which led to higher selectivity. Also, chlorin e6 exhibits a significantly higher efficiency in singlet oxygen generation when it is attached to a gold surface [66].

Similar research presenting applications of phthalocyanine derivatives conjugated to noble metal nanoparticles were presented by Ke *et al.* [67]. In this work, they attached tetra-substituted carboxyl aluminium phthalocyanine (AlC_4Pc) to the surface of gold nanorods coated with an SiO_2 layer. The distance between the AlC_4Pc moiety and the gold surface could be controlled by changing the thickness of the silica layer; the optimal distance was found to be 10.6 nm. Irradiation was carried out by a 680 nm LED lamp with an average power of 10 mW/cm^2 for 40 min. The formation of singlet oxygen monitored by ABDA showed that the concentration of singlet oxygen was 2.1 times higher for the composite particle than for the free AlC_4Pc solution. Another research group also used gold nanorods modified with AlPcS4 photosensitizer molecules [68]. The nanocomposite was investigated using a mode of high power density (short duration) combined with low power density (long duration) to reduce the damage to non-target cells (high 80 mW/cm^2, 0.5 min; low 25 mW/cm^2, 1.5 min). The intracellular efficacy of this high/low PDT mode in conjunction with the nanocomposite was assessed using an MTT assay in MCF-7 cancer cells. The high/low PDT achieved an extremely high efficacy, resulting in a cell mortality of over 90%.

Riboflavin has been identified as a highly efficient photosensitizer with high quantum yield (0.54) [69], and singlet oxygen generation can be enhanced by silver nanoparticles [70]. It has been reported that a 1.8-fold enhancement in singlet oxygen production can be attained compared to pure riboflavin (the generation of singlet oxygen was monitored by SOSG; excitation at a wavelength of 415 nm, average power of 31 mW). Since the system described has an absorption maximum at approximately 420 nm, its usage for clinical PDT is limited. However, it was shown that irradiating silver nanoparticles functionalized by pectine and riboflavine with 405 nm laser light (417 mW/cm^2) led to significant HeLa cell mortality [71].

Another nanocomposite for PDT is based on a silica-coated Au-Ag nanocage [72]. Metallic nanocages were prepared in ethylene glycol in the presence of sodium sulfide. The silica layer was prepared by decomposing tetraethyl orthosilicate in the presence of ammonia as a catalyst. The surface of the nanocomposite was then functionalized with amine groups using 3-aminopropyltriethoxysilane. Finally, the nanocomposite was mixed with an aqueous solution of Yb-2,4-dimethoxyhematoporphyrin (Yb–HP). Due to the electrostatic interaction between the positively charged amine groups on the particles and the carboxyl group of Yb-HP, the photosensitizer was adsorbed onto the surface of the nanoparticles. The nanocomposite exhibited a slightly lower efficiency than did the free Yb-HP molecules (irradiation at 633 nm, pulsed laser, average power 30 mW/cm^2). Nonetheless, the nanocomposite was sufficiently efficient to reduce the viability of HeLa cells, and could increase localization of the compound *in vivo*.

Gold nanoparticles loaded with IR780 exhibit singlet oxygen generation quantum yield on a level comparable to that of free IR780 [73]. However, in the case of Au@IR780, a photothermal effect was also observed, which improves the cytotoxicity against cancer cells.

Mitoxantrone encapsulated in gold hollow nanoparticles can also be activated by light [74]. It has been shown that the PEGylation process reduces absorption by proteins and provides a nanostructured surface as an amphiphilic environment for drugs that are insoluble in water. PEGylation also increases conjugation efficiency and reduces the unnecessary release of the drug. The nanocomposite obtained exhibits high biocompatibility. The nanocomposite was tested against a MCF-7 and DFW cells line, and it was shown that even a 3 μM concentration of the drug leads to over 70% cell death after light irradiation.

4.3. Semiconductor nanoparticles

It is also possible to use semiconductor nanoparticles as photosensitizers, provided that they have a higher energy band gap than that of singlet oxygen. The energy of the excitation light should be matched to the gap between the valence band and the conduction band. The energy of excitation can be transferred directly to an oxygen molecule in the ground state, or to an organic photosensitizer *via* a FRET mechanism.

Tungsten oxide nanowires have been used as a semiconductor photosensitizer, since the energy band gap in $W_{18}O_{49}$ nanowires is approximately 1.26 eV, which is higher than the 0.97 eV energy band gap of singlet oxygen, making energy transfer from the surface of the tungsten oxide to molecular oxygen possible [75]. The excitation of $W_{18}O_{49}$ was obtained after irradiation by 980 nm light, and the molar extinction coefficient was estimated to be 0.5×10^7, which is almost three orders of magnitude higher than the extinction coefficient of some organic photosensitizers. The nanowires were shown to be effective in treating B16F0 melanoma tumors in mice under low power laser irradiation (980 nm – 200 mW/cm^2), most probably by PDT, and not PTT.

Another very promising nanomaterial for PDT is graphene quantum dots – GQDs [76]. GQDs were prepared by the hydrothermal treatment of polythiophene. An *in vitro* cytotoxicity test was carried out on HeLa cells (excited with broad spectrum (400–800 nm) white light, power density 6.5 mW/cm^2). The efficacy of GQDs was compared with the organic photosensitizer PpIX. In these experiments, the HeLa cells were irradiated for 10 min with GQDs in concentrations ranging from 0.036 to 1.8 μM, and PpIX in concentrations ranging from 0.36 to 18 μM. Cell viability was reduced to 60% in the presence of 0.036 μM GQDs, and to 20% after incubation with 1.8 μM GQDs. Significantly lower cell viability was observed in the case of PpIX. A cell viability of 55% was obtained for the 1.8 μM PpIX solution under conditions of darkness, and more than 35% of the cells survived even after irradiation. In addition, the PpIX exhibited a higher cytotoxicity in dark conditions, whereas the GQDs exhibited low cytotoxicity and good biocompatibility. For the *in vivo* tests, groups of mice were intratumorally injected with GQDs at a concentration of 4 mg/kg, and were irradiated twice, on the first and seventh days, with 10 min of white light at an average power density of 80 mW/cm^2. A control group also received the same dose of GQDs but were not irradiated (C1 group), and a second control group did not receive GQDs but were irradiated (C2 group). In the PDT group, the tumour first turned black and festered. Decomposition of the tumour began after 17 days, and no tumour regrowth was observed even 50 days after treatment. In contrast, in both control groups tumour growth was significant during the experiment.

Typical semiconductor nanoparticles such as CdTe can also be used as photosensitizers for photodynamic therapy [77]. CdTe QDs were synthesized with 2-aminoethanethiol as a surface stabilizer, and the surface was then modified with meso-tetra(4-sulfonatophenyl)porphine dihydrochloride (TSPP) due to electrostatic interaction. Depositing TSPP on the surfaces of the CdTe quantum dots led to a shift in the luminescence maximum into the blue region. The extinction coefficient of the nanocomposite at 355 nm was estimated to be 18 300 M^{-1} cm^{-1}. Excitation of the nanocomposite with a Nd:YAG laser at 355 nm caused a characteristic phosphorescence from singlet oxygen at 1270 nm. No singlet oxygen was observed when the CdTe quantum dots were excited in the absence of TSPP. The quantum yield of the process was estimated to be 0.43 at a wavelength where the absorption of photosensitizers is minimal. It was therefore suggested that the generation of singlet oxygen after excitation of the CdTe quantum dots took place by a FRET mechanism. However, the presence of the heavy metal cadmium in the nanocomposite significantly reduces its applicability for clinical PDT. Similar systems based on TiO_2 quantum dots have been developed using hypocrellin B (HB) to modify the surface [78]. Hypocrellin is a natural pigment with an absorption band in the visible region. The quantum yield of singlet oxygen generation for free HB was estimated to be 0.76. However, the formation of an HB-TiO_2 nanocomposite led to an increase in the quantum yield to 0.86. The HB-TiO_2 nanocomposite was irradiated by a pulsed laser at 532 nm, and the generation of singlet oxygen was monitored using TEMP. The formation of the HB-TiO_2 nanocomposite led to a shift in the absorption maximum from the UV to the visible range.

ZnO quantum dots with an average diameter of 11.6 nm have been shown to produce singlet oxygen and other reactive oxygen species such as the hydroxyl radical ($^{\cdot}OH$) and superoxide anion ($^{\cdot}O_2^-$), after irradiation with blue (400–500 nm) light [79]. The singlet oxygen sensor was used, and a characteristic EPR triplet spectrum of TEMPO was detected after irradiation of the ZnO nanoparticles by blue light. In the non-irradiated samples of ZnO, no triplet signal was detected.

Another way to use quantum dots for PDT is in core-shell nanostructures, such as CdSe/CdS/ZnS stabilized by dihydrolipoic acid derivatives (amine-DHLA) [80]. In the example, due to the positive charge of the DHLA organic photosensitizer on the surface of the quantum dots, the negatively-charged sulfonated aluminium phthalocyanines (AlPcS) were able to bind. The nanocomposites were irradiated with 532 nm laser light in the presence of DPBF as a sensor for singlet oxygen. No singlet oxygen production could be recorded for free AlPcS molecules, because this organic photosensitizer does not absorb light at 532 nm. Therefore, the generation of singlet oxygen in the presence of QDs is based on a FRET mechanism. The results obtained showed that AlPcS-QDs under 532 nm laser irradiation produced cell death in nasopharyngeal (KB) carcinoma cells. Very similar nanocomposites were proposed by another research group [81] using the same type of quantum dots (CdSe/CdS/Zns) but using the organic photosensitizer Rose Bengal (RB), and chlorin e6. The quantum yield of the generation of singlet oxygen was estimated on 0.17 for the QD-RB conjugates and 0.31 for the QD-chlorin e6 conjugates (using an Nd:YAG laser; excitation at 532 nm). Alternatively, Nitrogen-Doped Graphene Quantum Dots can also be coupled with Rose Bengal [82] or aluminum tetrasulfonated phthalocyanine (ClAlTSPc) [83] to obtain an efficient nanosystem for singlet oxygen generation. Another system is based on core-shell quantum dots, conjugated CdSe/ZnS with an iridium complex ([(piq)$_2$Ir(L2)]) [84]. A strong phosphorescence signal from

oxygen in the excited state can be observed during illumination by 514 nm laser light.

Very promising nanosystems for PDT could be based on Ag_2S quantum dots, due to their emission band in the NIR biological window [85]. It has been reported that Ag_2S quantum dots exhibit high biocompatibility and negligible toxicity in terms of cell proliferation, apoptosis and necrosis, ROS, and DNA damage.

4.4. Functionalised silica nanospheres

While silica itself is not active for PDT, the encapsulation of photosensitizers within silica nanoparticles is very promising, since silica is nontoxic, chemically inert, and optically transparent. Furthermore, the hydroxyl groups on the silica surface make chemical functionalization easy. In the literature, silica nanoparticles are largely described for use as a material for drug delivery. In 2008, Rossi et al. described silica nanoparticles loaded with Protoporphyrin IX (Pp IX) as a novel anticancer system [86]. The generation of singlet oxygen was carried out by directly measuring the phosphorescence of singlet oxygen after irradiation at 532 nm, and using DBPF as a sensor. It was observed that the quantum yield of singlet oxygen was higher when the silica nanoparticles were loaded with PpIX than for the free protoporphyrin solution. Another nanosystem for PDT based on silica nanospheres was presented by Yan & Kopelman [87]. They reported that embedding meta-tetra(hydroxyphenyl)-chlorin (m-THPC) into silica nanoparticles caused a positive effect on the production of singlet oxygen. It was determined that the reaction rates constant with ADPA for free m-THPC and m-THPC embedded in silica NP were $2.73{\cdot}10^8$ M^{-1} s^{-1} and $4.83{\cdot}10^8$ M^{-1} s^{-1}, respectively.

Encapsulation in silica may also protect compounds from enzymatic degradation; this was demonstrated using methylene blue (MB) [88]. Silica MB nanocomposites were incubated with HeLa cells and exposed to 635 nm laser light at an average power of 27.5 mW/cm^2 for 45 min, and singlet oxygen generation monitored using DPBF. The MB-encapsulated SiO_2 NPs were tested at concentrations of 7, 3.5, 1, 0.7 mg/ml, and all showed cell death rates higher than 80%. In the presence of the nanocomposite (1 mg/ml and 0.7 mg/ml), but in the absence of excitation light, less than 20% of the cells were killed, which indicates that the dark cytotoxicity was relatively low. Higher concentrations of the nanocomposite resulted in a high dark cytotoxicity. It was concluded that a concentration of 1 mg/ml was the optimal concentration for effective photocytotoxicity under laser irradiation with little dark cytotoxicity.

Silica encapsulation has been also used to enhance the photodynamic efficacy of Pc4 [89]. It is well known that free Pc4 molecules aggregate in aqueous systems, resulting in decreased singlet oxygen production. Pc4 encapsulation by silica nanoparticles protects the Pc4 molecule from aggregation and thus shows a higher singlet oxygen production than free Pc4. The silica Pc4 nanocomposite was used against A375 and B16F10 melanoma cells. It was reported that more than half of the cells were destroyed after irradiation of the nanocomposite, even at concentrations below 5 nM. The photo-stability, generation of singlet oxygen, and therapeutic efficacy of the photosensitizer Pc4 were significantly improved by encapsulation into porous silica nanoparticles. In a similar system, hematoporphyrin was incorporated into the walls of hollow mesoporous silica nanoparticles [90]. This system achieved high biocompatibility and low dark cytotoxicity even at high concentrations (200 μg/ml). The photodynamic activity was tested against an MCF-7 cell line, with positive results.

A further innovation incorporated MB into silica-coated magnetic particles [91,92]. The particles showed a blue-shift in the maximum absorption of MB from 664 nm (in water) to 590 nm after immobilization in the silica matrix. This shift may have been connected with the aggregation and demethylation of the MB molecules. After irradiation of the nanoparticles (Nd:YAG laser; 532 nm), singlet oxygen was detected directly from the fluorescence at 1270 nm and using DPBF as a sensor. However, a significant decrease was observed in the quantum yield of singlet oxygen generation after the incorporation of the photosensitizer molecules into the silica layer.

It was also reported that silica nanospheres decorated with chlorin e6 and folic acid can efficiently generate singlet oxygen after laser illumination [93]. It was observed that the *in vitro* application of such nanoparticles led to apoptosis of the targeted cells. Another study showed that not only silica nanospheres, but also titania, can be conjugated with chlorin e6, [94].

4.5. Upconversion nanoparticles

Photon upconversion is a process in which the sequential absorption of two or more photons leads to the emission of light at a shorter wavelength than the excitation wavelength [95]. Such an anti-Stokes emission can, for example, convert infrared light to visible light [96]. It has been reported that upconversion nanoparticles such as $NaYF_4$ could be applied in PDT. Upconversion nanoparticles can be excited by low energy light from the NIR region, and two or three photons transferred into one photon with higher energy; the emitted photon can then excite an organic photosensitizer. Generally, in upconversion nanosystems for PDT, smaller mismatches between the absorption band of photosensitizer and the emission band of the upconversion nanoparticles (UCNP) lead to a higher efficiency of $^1O_2$ generation. The first demonstration of upconversion nanocomposites for PDT was presented in 2007 by Zhang et al. [97]. They observed that $NaYF_4$:Yb^{3+},Er^{3+} nanoparticles could be excited by IR light (974 nm) and exhibit two strong emission bands in the visible region at 537 nm and 635 nm. The surface of the particles was coated with silica, and the photosensitizer Merocyanine 540 (M-540) was attached. M-540 had been previously used in PDT as a photosensitizer with a visible light source [98]. The generation of singlet oxygen was confirmed by a decrease in the fluorescence emission of the sensor ADPA. Due to the good match between the absorption band of the photosensitizer and the emission band of the upconversion nanoparticles, the nanocomposite was used successfully to kill MCF-7/AZ breast cancer cells.

A similar system has included gadolinium to generate $NaYF_4$:Er/Yb/Gd upconversion nanocrystals. These were then conjugated with methylene blue [99]. Methylene blue exists in dimer and monomer forms that exhibit absorption maxima at 600 and 660 nm, respectively. The $NaYF_4$:Er/Yb/Gd nanocrystal exhibits a red emission peak at 651 nm, and therefore the absorption/emission mismatch between the UCNP and the dye is less than 5 nm. Nanocomposites were irradiated with 980 nm laser light in the presence of DPBF as a sensor for singlet oxygen. The control experiment confirmed that no signal was seen for either $NaYF_4$:Er/Yb/Gd alone, or free methylene blue solutions. A similar system was based on $NaYF_4$:Yb,Er conjugated with another organic photosensitizer - Rose Bengal [100,101] or $NaYF_4$:Yb/Er conjugated with Vitamin B_{12} [102].

$NaYF_4$:Yb,Er (Y:Yb:Er 78%:20%:2%) nanoparticles have been also combined with the photosensitizer chlorin e6 (Ce6) [103]. The UCNP was excited by 984 nm laser light, and exhibited two emission bands, at 550 and 660 nm. The emission band at 660 nm was well matched with the absorption peak of Ce6. *In vivo* experiments were carried out on mice with 4T1 murine breast tumor xenografts. Upconversion nanoparticles were intratumorally injected and irradiated with NIR light. Each group used 40–50 μl of upconversion nanoparticles or saline (control group) and was exposed for 30 min with 980 nm laser light with an average power density of 0.5 W/cm^2. The results showed that, in the case of the nanocomposites combined with NIR light, the tumour cells were completely destroyed and no tumour regrowth was observed even after 60 days. The control samples showed no obvious damage to the tumour cells. A similar nanocomposite based on $NaYF_4$ upconversion nanoparticles with another organic photosensitizer, zinc(II)-phthalocyanine (ZnPc), was tested against MB-49-PSA bladder cancer cells [104]. It was confirmed that more $^1O_2$ was produced in the cells

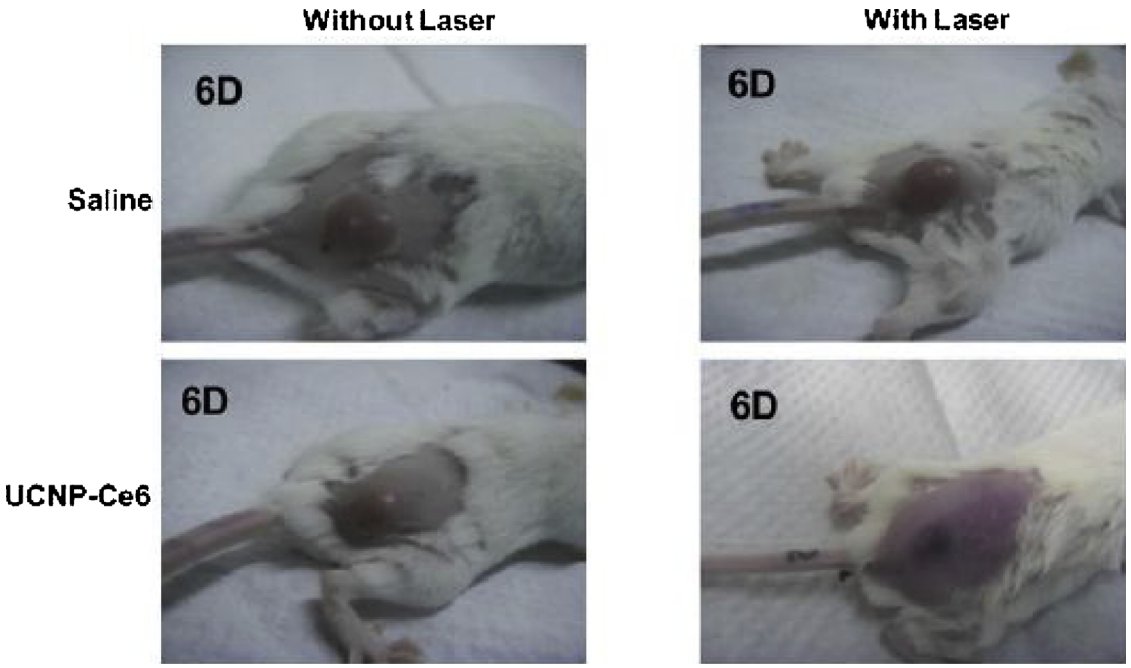

Fig. 12. Photos of mice after 6th days of PDT treatment in various conditions after application of UCNP-Ce6. Reprinted with permission from ref. [80]. Copyright 2011 Elsevier.

treated by the upconversion nanoparticles conjugates with ZnPc than in those with free nanoparticles of free ZnPc molecules. $NaYF_4$ nanoparticles doped with Yb^{3+} and Er^{3+} have also been conjugated with ZnPC [105]. These were successfully applied against human alveolar adenocarcinoma (A549) cells. $NaYF_4$ upconversion nanoparticles have been also conjugated with Rose Bengal (RB) [106]. Upconversion nanoconjugates were excited by 980 nm laser light, and the generation of singlet oxygen was monitored using DPBF as a sensor, showing phosphorescence of $^1O_2$ at 1270 nm. The upconversion nanocomposite was tested against choriocarcinoma (JAR) cells. It was observed that the nanoconjugates were mainly localized in the cytoplasm and perinuclear regions of the cells. Before excitation, no significant morphological changes were observed in the cancer cells, suggesting good biocompatibility. After illumination, cell viability decreased significantly, and was related to the concentration of nanoconjugates.

An alternative upconversion nanocomposite $LiYF_4$:Tm^{3+}/Yb^{3+} showed stronger blue emission after NIR excitation than a similar $NaYF_4$ upconversion nanocomposite [107]. In order to generate singlet oxygen, the surfaces of the $LiYF_4$:Tm^{3+}/Yb^{3+} nanoparticles were modified with 5,10,15,20-tetra(m-hydroxyphenyl)-chlorin (m-THPC), and singlet oxygen was detected after excitation by 980 nm laser light. *In vitro* tests were carried out on the HeLa cells, and the nanocomposite showed no intrinsic toxicity towards the cells when not irradiated. The excitation of particles ranging in a concentration of from 0.5-2.50 μM in the cells, resulted in a cell death of between 20% and 70% after irradiation for one hour.

In similar studies, $NaYF_4$:Yb,Er upconversion nanoparticles was conjugated with zinc phthalocyanine (ZnPc) [108]. Singlet oxygen was detected by DPBF after irradiation with 980 nm laser light. Photodynamic activity was tested in the HeLa and A549 cells. The cells were irradiated for 10 min with different light power densities, and cell viability was measured using an MTT assay. It was reported that the $NaYF_4$:Yb,Er upconversion nanoparticles - ZnPc nanocomplex exhibited low dark cytotoxicity even at concentrations of 200 μg/ml, while the optimal power density of the laser beam was estimated to be 0.39 W/cm^2. Under these conditions, the viability of the HeLa cells was estimated to be 30%. Such nanocomplex was also intratumorally injected into Hepa1-6 tumor-bearing C57/6 J mice. The tumors were irradiated with 980 nm laser light (0.39 W/cm^2) for 15 min. It was observed that there was significant inhibition of tumor growth and a reduction in tumor volume (see Fig. 12). Mice from the control group did not show any therapeutic effects. A histological analysis did not reveal any pathological changes in the heart, lung, kidney, liver or spleen. Hepatocytes in the liver samples were found normal.

Upconversion nanoparticles have been also prepared with a coating of mesoporous silica layer into which the organic photosensitizer ZnPc was incorporated [109]. This resulted in a colour change of the upconversion nanoparticles from white to blue after ZnPc incorporation. The mesoporous silica can protect encapsulated photosensitizer molecules from degradation in a harsh biological environment. The generation of singlet oxygen was monitored by ABDA, and in solutions containing $NaYF_4$ nanoparticles without ZnPc molecules, the fluorescence spectrum of ABDA remained unchanged during illumination. Those particles in which ZnPc was incorporated into a silica layer around the upconversion nanoparticles showed a significant decrease in the peak intensity at 431 and 380 nm, indicating the formation of singlet oxygen. The nanocomposites were incubated with MB49-PSA cells at a final concentration of 100 μM, and cell viability estimated to be reduced to 30%. Another nanocomposite comprised AlC4PC molecules incorporated into $NaGdF_4$:Yb,Er@SiO_2 [110]. This nanocomposite was irradiated with 980 nm laser light in the presence of DPBF as sensor for singlet oxygen. In the presence of UCNP@SiO_2 - AlC4Pc nanoparticles, the DPBF absorption band at 400 nm dramatically decreased under 980 nm laser irradiation. Solutions containing only upconversion nanoparticles covered with a SiO_2 layer, or free AlC4Pc, showed no decrease in the DPBF absorption band. The nanocomposite was tested *in vitro* against MEAR cells; irradiation with a 980 nm laser (average power density 0.5 W/cm^2, for 2 or 5 min) showed that almost 40% of cells were killed after 5 min of irradiation (Fig. 13).

$NaYF_4$:Yb,Tm upconversion nanoparticles have been coated with a nanometric layer of silica, functionalized with amino groups after incubation with APTES, and covalently bound to the organic photosensitizer Ce6 via the amino groups on the silica layer [111]. Photodynamic activity was tested *in vitro* against the MCF-7 human breast adenocarcinoma cell line. The upconversion nanoparticle-Ce6 nanocomplex (50 μg/ml) was irradiated for 10 min with 980 nm laser light,

and half of the cells were killed. In the unilluminated sample, cytotoxicity was very low; cell viability was greater than 90%.

Alternatively, it has been shown that $NaGdF_4$:Yb,Er upconversion nanoparticles can be applied for dual photosensitizer photodynamic therapy [112]. In this case, upconversion nanoparticles were conjugated with chlorin e6 and MC540. Overlaps of the absorption band of each of the photosensitizers with the emission band of the upconversion nanoparticles led to a significantly higher efficiency of singlet oxygen generation.

The well-studied photocatalyst titanium dioxide has been also used in combination with upconversion nanoparticles. TiO_2 exhibits high phototoxicity towards cancer cells upon irradiation by UV light. However, the limited penetration of UV light through human tissue significantly reduces its applicability. An interesting solution was presented by Lucky et al. [113], wherein $NaYF_4$:Yb,Tm nanoparticles were coated with a TiO_2 layer. In the control experiments, continuous irradiation of OSCC (Oral Squamous cell carcinoma) cells with 980 nm laser light at an average power density of 2.1 W/cm^2 for 320 s showed greater than 95% cell viability. Under the same conditions, in the presence of 2 mM upconversion nanoparticles covered with a TiO_2 layer, irradiation led to cell death in more than 80% of the cells. Under the same conditions, without irradiation, there was good biocompatibility and low dark cytotoxicity. The nanocomposite was tested *in vivo* on mice. The results showed that PDT treatment based on upconversion nanoparticles covered with a TiO_2 layer could be used as a safe therapeutic procedure. During the experiment, there was no significant decrease in the body weight in any of the animals treated. In the control animal groups treated by NIR light alone, or upconversion nanoparticles covered with a TiO_2 layer without NIR irradiation, there was no therapeutic effect. When incubated with upconversion nanoparticles covered with a TiO_2 layer, exposure to NIR light resulted in a significant delay in tumor growth. However, in the case of a single PDT regimen, complete tumor inhibition was not observed. It is possible that a second round of PDT, 2 weeks after the first dose, when the residual tumor starts to regrow, could result in better control of tumor growth and prevent a relapse.

Upconversion nanoparticles can be coupled with graphene quantum dots in order to improve photodynamic therapy efficiency [114]. The graphene quantum dots exhibited an absorption peak at 340 nm, which matched well with the emission band of upconversion nanoparticles at 336 and 363 nm after irradiation with 980 nm laser light. Singlet oxygen generation was monitored in presence of DPBF and SOSG as a sensor. As the light source, a 980 nm laser beam at an average power of 1.5 W/cm^2 was used. It was found that the upconversion nanoparticle-GQD complex exhibited good biocompatibility; even in the case of high nanoparticle concentration, cell viability was higher than 90%. Photodynamic activity was tested against the 4T1 cell line. After irradiation by laser light, cell viability was significantly lower. The nanosystem described was also tested *in vivo* in 4T1 tumor-bearing BALB mice. The results showed much slower growth rates, indicating excellent tumor inhibition efficacy, with the tumor inhibition rate estimated to be higher than 70%. A similar approach was taken by S.Y. *Choi et al.* [115]; however, the surfaces of the graphene quantum dots were functionalized by Hypocrellin A (HA) in order to enhance singlet oxygen generation.

Upconversion nanoparticles can be also modified by introducing a magnetic core into them [116], or by adding another magnetic species [117,118], which simplifies the accumulation of nanoparticles in diseased tissue.

Summary of application of nanoparticles in PDT in various experimental conditions

Nanoparticles	Laser wavelenght [nm]	Power intensity	Method of detection	Target cells	Ref
Au nanorods	915	130 mW/cm^2	SOSG	B16F0	46
Au nanoechinus	940	130 mW/cm^2	SOSG	HeLa	44
Au bipyramids	660, 710, 820, 930	200 mW/cm^2	ABDA	HeLa	49
Aggregated Au nanoparticles	800	3 W/cm^2	ABDA	–	50
Au nanoshell	808	150 mW/cm^2	direct phosphorescence at 1063nm	Hela	45
	980		SOSG	B16F0	
Ag nanoprisms	544	45 mW/cm^2	SOSG, hydroperoxidation of cyclohexene	–	42
Ag decahedrons	885	66 mW/cm^2			
Au nanostar@SiO_2@methylene blue	633	700 mW/cm^2	SOSG	BT549	52
Ag@riboflavin	415	31 mW	SOSG	–	57
Au-Ag nanocage@Yb-HP	633	30 mW/cm^2	–	HeLa	59
Au@SiO_2@AlC4Pc	680	10 mW/cm^2	ABDA	–	55
Ag@SiO_2@PpIX	halogen white lamp	30 W	TEMP	–	43
$Au_{25}(capt)_{18}$- cluster	650	13 mW/cm^2	DAB	Hela	51
	808	41 mW/cm^2			
$W_{18}O_{49}$ nanorods	980	200 mW/cm^2	SOSG	B16F0	60
Graphene QDs	white lamp	6.5 mW/cm^2	ADPA	HeLa	61
CdTe – TSPP	355	–	direct phosphorescence at 1063nm	–	62
$NaYF_4$:Yb^{3+}/Er^{3+} – M-540	974	–	ADPA	MCF-7/AZ	78
$NaYF_4$:Er^{3+}/Yb^{3+}/Gd^{3+} – MB	980	–	DPBF	–	79
$NaYF_4$ Y^{3+}/Yb^{3+}/Er^{3+} – Ce6	984	–	–	4T1	80
$NaYF_4$ Yb^{3+}. Er^{3+}/- RB	980	–	–	A549	82
$LiYF_4$:Tm^{3+}/Yb^{3+} – m-THPC	980	–	–	HeLa	73

4.6. Nanoparticles for PDT activated by X-ray radiation

All the above-described nanoparticles and nanocomposites can be activated by laser or LED light. However, some nanoparticles can also be activated by X-ray radiation. For this purpose, various kind of nanoparticles can be used: transition metal nanoparticles [119–122], quantum dots [123,124] or noble metal nanoparticles [125]. However, because they are activated by X-ray radiation, such systems are not described in detail in this work.

5. Conclusions

In this article we described the applications of various nanoparticles that can be used for photodynamic therapy (PDT), and possible methods of detecting the singlet oxygen generated. Plasmonic nanoparticles exhibit a number of desirable properties for use in PDT. Firstly, they are able to generate singlet oxygen during irradiation with light in a range between 800 and 1000 nm, where human tissue exhibits a transparency window. In comparison with typical organic photosensitizers such as hematoporphyrins, they exhibit higher photostability and resistance to enzymatic degradation. Also, their higher excitation coefficients make a reduction in the power of the excitation light possible. Upconversion nanoparticles also make excitation by NIR light

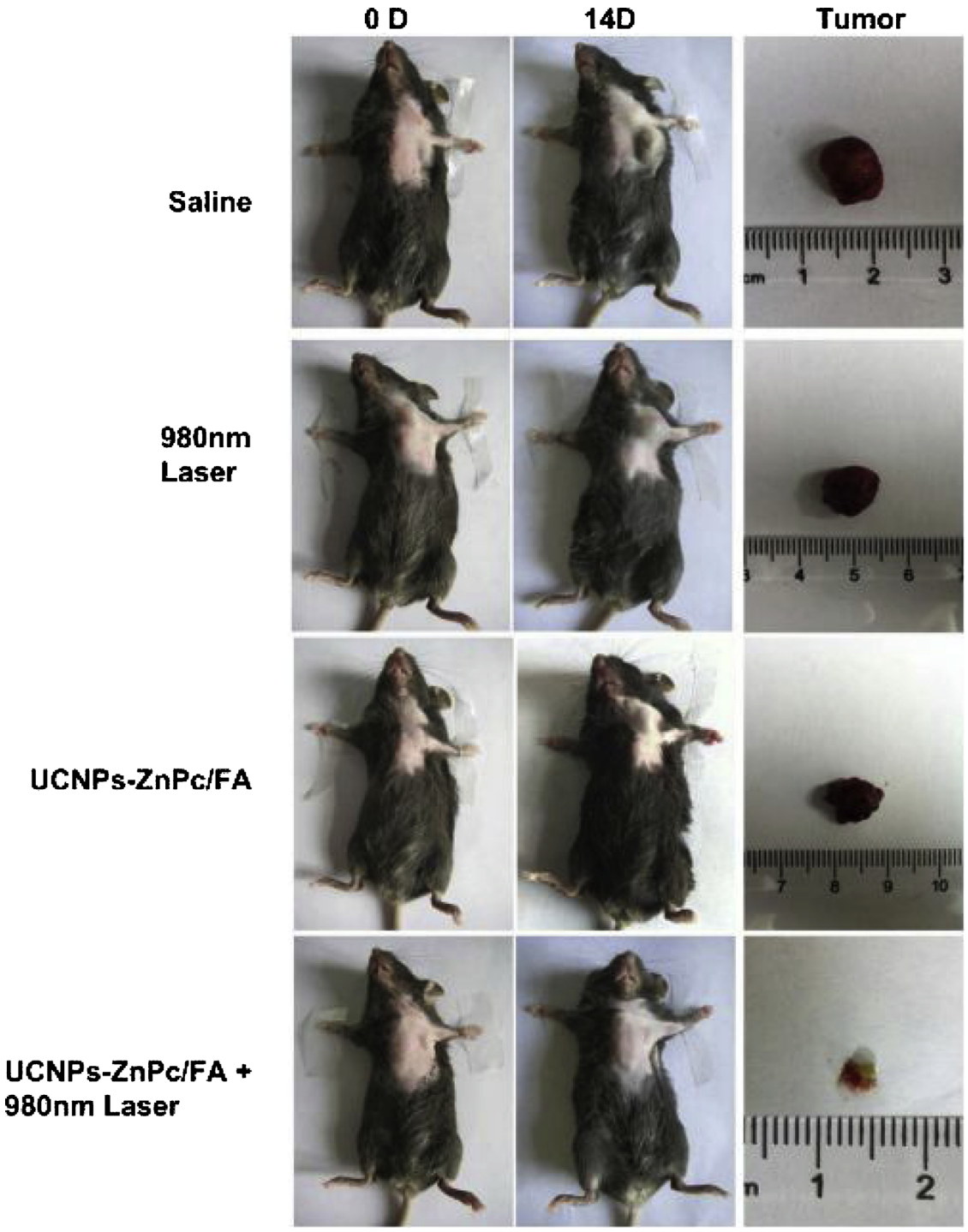

Fig. 13. Photos of mice and liver tumor before and after various PDT treatments based on $NaYF_4$:Yb,Er upconversion nanoparticles -ZnPc nanocomplex, and photos of tumor tissue obtained after 14 days. Reprinted with permission from ref. [84]. Copyright 2014 Elsevier.

possible, and emissions at shorter wavelengths that are compatible with organic photosensitizers. Quantum dots are another possibility for use in PDT, although at present they have less than optimal properties for clinical applications. Their main disadvantages are the presence of heavy metals, which are potentially toxic, and an absorption band in the visual region of the spectrum (400–500 nm), where penetration of light through tissues is not high. It is expected that, due to their very promising optical properties, plasmonic nanoparticles, plasmonic composites, and upconversion nanoconjugates will have a significant impact on the detection and treatment of cancer in the near future.

Conflict of interest

On behalf of all authors, the corresponding author states that there is no conflict of interest.

Acknowledgments

This work was financed out of funds of the National Science Centre, Poland, No. UMO-2017/24/T/ST5/00171

References

[1] F. Meyer–Betz, Investigations on the biological (photodyanmic) action of hematoporphyrin and other derivatives of the blood and bile pigments, Arch. Klin. Med. 112 (1913) 476–503.

[2] S.K. Schwartz, K. Abolon, H. Vermund, Ome relationships of porphyrins, X-rays and tumors, Univ. Minn. Med. Bull. 27 (1955) 7–8.

[3] R.L. Lipson, E.J. Baldes, A.M. Olsen, The use of a derivative of hematoporhyrin in tumor detection, J. Natl. Cancer Inst. 26 (1961) 1–11.

[4] R.L. Lipson, E.J. Baldes, The photodynamic properties of a particular hematoporphyrin derivative, J. Arch. Dermatol 82 (4) (1960) 508–516 https://508–516,10.1001/archderm.1960.01580040026005.

[5] I. Diamond, S.G. Granelli, A.F. McDonagh, S. Nielsen, C.B. Wilson, R. Jaenicke, Photodynamic therapy of malignant tumours, Lancet 2 (2) (1972) 1175–1177, https://doi.org/10.1016/S0140-6736(72)92596-2.

[6] T.J. Dougherty, G.B. Grindey, R. Fiel, K.R. Weishaupt, D.G. Boyle, Photoradiation therapy. II. Cure of animal tumors with hematoporphyrin and light, J. Natl. Cancer Inst. 55 (1) (1975) 115–121.

[7] J.F. Kelly, M.E. Snell, M.C. Berenbaum, Photodynamic destruction of human bladder carcinoma, Br. J. Cancer 31 (2) (1975) 237–244.

[8] J.F. Kelly, M.E. Snell, Hematoporphyrin derivative: a possible aid in the diagnosis and therapy of carcinoma of the bladder, J. Urol. 115 (2) (1976) 150–151, https://doi.org/10.1016/S0022-5347(17)59108-9.

[9] Y. Hayata, H. Kato, C. Konaka, J. Ono, N. Takizawa, Hematoporphyrin derivative and laser photoradiation in the treatment of lung Cancer, Chest 81 (3) (1982) 269–277, https://doi.org/10.1378/chest.81.3.269.

[10] O.J. Balchum, D.R. Doiron, G.C. Huth, Photoradiation therapy of endobronchial lung cancers employing the photodynamic action of hematoporphyrin derivative, Lasers Surg. Med. 4 (1) (1984) 13–30, https://doi.org/10.1002/lsm.1900040104.

[11] Y. Hayata, H. Kato, H. Okitsu, M. Kawaguchi, C. Konaka, Photodynamic therapy with hematoporphyrin derivative in cancer of the upper gastrointestinal tract, Semin. Surg. Oncol. 1 (1) (1985) 1–11, https://doi.org/10.1002/ssu.2980010103.

[12] D.R. Sandeman, Photodynamic therapy in the management of malignant gliomas: a review, Lasers Med. Sci. 1 (3) (1986) 163–167, https://doi.org/10.1007/BF02040233.

[13] J.S. Hill, A.H. Kaye, W.H. Sawyer, G. Morstyn, P.D. Megison, S.S. Stylli, S.K. Powers, J.E. Boggan, Selective uptake of hematoporphyrin derivative into human cerebral glioma, Neurosurgery 26 (2) (1990) 248–254, https://doi.org/10.1227/00006123-199002000-00011.

[14] E.A. Popovic, A.H. Kaye, J.S. Hill, Photodyanmic therapy of brain tumors, J. Clin. Laser Med. Surg. 14 (1996) 251–261 https://10.1089/clm.1996.14.251.

[15] M.A. Rosenthal, B. Kavar, J.S. Hill, D.J. Morgan, R.L. Nation, S.S. Stylli, R.L. Basser, S. Uren, H. Geldard, M.D. Green, S.B. Kahl, A.H. Kayeet, Phase I and pharmacokinetic study of photodynamic therapy for high-grade gliomas using a novel boronated porphyrin, J. Clin. Oncol. 19 (2) (2001) 519–524, https://doi.org/10.1200/JCO.2001.19.2.519.

[16] V.G. Schweitzer, Photodynamic therapy for treatment of head and neck cancer, Otolaryngol. Head Neck Surg. 102 (1990) 225–232.

[17] M.A. Biel, Photodynamic therapy and the treatment of head and neck neoplasia, Laryngoscope 108 (9) (1998) 1259–1268, https://doi.org/10.1097/00005537-199809000-00001.

[18] P. Mlkvy, H. Messmann, J. Regula, M. Conio, M. Pauer, C.E. Millson, A.J. MacRobert, S.G. Bown, Photodynamic therapy for gastrointestinal tumors using three photosensitizers - ALA induced PPIX, Photofrin® and MTHPC. A pilot study, Neoplasma 45 (3) (1998) 157–161.

[19] J.P. Tardivo, A. Giglio, C.S. De Oliveira, D.S. Gabrielli, H.C. Junqueira, D.B. Tada, D. Severino, R. Turchiello, M.S. Baptista, Methylene blue in photodynamic therapy: from basic mechanisms to clinical applications, Photodiagn. Photodyn. Ther. 2 (3) (2005) 175–191, https://doi.org/10.1016/S1572-1000(05)00097-9.

[20] J.J.M. Lamberts, D.C. Neckers, Rose Bengal derivatives as singlet oxygen sensitizers, Tetrahedron 41 (11) (1985) 2183–2190, https://doi.org/10.1016/S0040-4020(01)96591-3.

[21] E. Gandin, Y. Lion, A. Van de Vorst, Quantum yield of singlet oxygen production by xanthene derivatives, Photochem. Photobiol. 37 (3) (1983) 271–278, https://doi.org/10.1111/j.1751-1097.1983.tb04472.x.

[22] H.C. Junqueira, D. Severino, L.G. Dias, M.S. Gugliottia, M.S. Baptista, Modulation of methylene blue photochemical properties based on adsorption at aqueous micelle interfaces, Phys. Chem. Chem. Phys. 4 (11) (2002) 2320–2328, https://doi.org/10.1039/B109753A.

[23] D. Severino, H.C. Junqueira, M. Gugliotti, D.S. Gabrielli, M.S. Baptista, Influence of negatively charged interfaces on the ground and excited state properties of methylene blue, Photochem. Photobiol. 77 (5) (2003) 459–468, https://doi.org/10.1562/0031-8655(2003)0770459IONCIO2.0.CO2.

[24] M.C. De Rosa, R.C. Crutchley, Photosensitized singlet oxygen and its applications, Coord. Chem. Rev. 233/234 (2002) 351–371, https://doi.org/10.1016/S0010-8545(02)00034-6.

[25] W. Spiller, D. Wöhrle, G. Schulz-Ekloff, W.T. Ford, G. Schneider, J. Stark, Photooxidation of sodium sulfide by sulfonated phthalocyanines in oxygen-saturated aqueous solutions containing detergents or latexes, Photochem. Photobiol. A: Chem. 95 (2) (1996) 161–173, https://doi.org/10.1016/1010-6030(95)04248-2.

[26] R.R. Allison, C.H. Sibata, Oncologic photodynamic therapy photosensitizers: a clinical review, Photodiagn. Photodyn. Ther. 7 (2010) 61–75, https://doi.org/10.1016/j.pdpdt.2010.02.001.

[27] J.D. Breskey, S.E. Lacey, B.J. Vesper, W.A. Paradise, J.A. Radosevich, M.D. Colvard, Photodynamic therapy: occupational hazards and preventative recommendations for clinical administration by healthcare providers, Photomed. Laser Surg. 31 (2013) 398–407, https://doi.org/10.1089/pho.2013.3496.

[28] P.J. Lou, H.R. Jager, L. Jones, T. Theodossy, S.G. Bown, C. Hopper, Interstitial photodynamic therapy as salvage treatment for recurrent head and neck cancer, Br. J. Cancer 91 (2004) 441–446, https://doi.org/10.1038/sj.bjc.6601993.

[29] P. Hervé Brun, J.L. DeGroot, E.F. Gudgin Dickson, M. Farahanib, R.H. Pottier, Determination of the in vivo pharmacokinetics of palladium-bacteriopheophorbide (WST09) in EMT6 tumour-bearing Balb/c mice using graphite furnace atomic absorption spectroscopy, Photochem. Photobiol. Sci. 3 (11) (2004) 1006–1010.

[30] M.J. Steinbeck, A.U. Khan, M.J. Karnovsky, Intracellular singlet oxygen generation by phagocytosing neutrophils in response to particles coated with a chemical trap, J. Biol. Chem. 267 (19) (1992) 13425–13433.

[31] G.R. Martines, J.L. Ravanat, M.H.G. Medeiros, J. Cadet, P.D. Mascio, Synthesis of a naphthalene endoperoxide as a source of 18O-labeled singlet oxygen for mechanistic studies, J. Am. Chem. Soc. 122 (41) (2000) 10212–10213 https://10.1021/ja0016452.

[32] G.R. Martinez, J.L. Ravanat, J. Cadet, S. Miyamoto, M.H.G. Medeiros, P.D. Mascio, Direct evidence of singlet molecular oxygen [O2 (1Δg)] production in the reaction of linoleic acid hydroperoxide with peroxynitrite, J. Am. Chem. Soc. 125 (15) (2004) 3056–3057 https://10.1021/ja029262m.

[33] M. Borsivall, D.F. Evans, A new trap for singlet oxygen in aqueous solution, J. Chem. Soc. Chem. Comm 0 (24) (1979) 1114–1116 https://10.1039/C39790001114.

[34] V. Nardello, J.M. Aubry, P. Johnston, I. Bulduk, A.H.M. de Vries, P.L. Alsters, Facile preparation of the water-soluble singlet oxygen traps Anthracene-9,10-divinylsulfonate (AVS) and Anthracene-9,10-diethylsulfonate (AES) via a heck reaction with vinylsulfonate, Synlett 17 (2005) 2667–2669, https://doi.org/10.1055/s-2005-917104.

[35] V. Nardello, J.M. Aubry, Synthesis and properties of a new cationic water-soluble trap of singlet molecular oxygen, Tetrahedron Lett. 38 (42) (1997) 7361–7364, https://doi.org/10.1016/S0040-4039(97)10018-1.

[36] G.R. Martinez, F. Garcia, L.H. Catalani, J. Cadet, M.C.B. Oliverira, G.E. Ronsein, S. Miyamoto, M.H.G. Medeiros, P.D. Mascio, Synthesis of a hydrophilic and non-ionic anthracene derivative, the N,N′-di-(2,3-dihydroxypropyl)-9,10-anthracene-dipropanamide as a chemical trap for singlet molecular oxygen detection in biological systems, Tetrahedron 62 (46) (2006) 10762–10770, https://doi.org/10.1016/j.tet.2006.08.094.

[37] V. Nardello, N. Azaroual, I. Cervoise, G. Vermeersch, J.M. Aubry, Synthesis and photooxidation of sodium 1,3-cyclohexadiene-1,4-diethanoate: a new colorless and water-soluble trap of singlet oxygen, Tetrahedron 52 (6) (1996) 2031–2046, https://doi.org/10.1016/0040-4020(95)01004-1.

[38] K. Tanaka, T. Miura, N. Umezawa, Y. Urano, K. Kikuchi, T. Higuchi, T. Nagano, Rational design of fluorescein-based fluorescence probes. Mechanism-based design of a maximum fluorescence probe for singlet oxygen, J. Am. Chem. Soc. 123 (11) (2001) 2530–2536 https://10.1021/ja0035708.

[39] C. Flors, M.J. Fryer, J. Waring, B. Reeder, U. Bechtold, P.M. Mullineaux, S. Nonell, M.T. Wilson, N.R. Baker, Imaging the production of singlet oxygen in vivo using a new fluorescent sensor, Singlet Oxygen Sensor Green, J. Exp. Bot. 57 (8) (2006) 1725–1734 https://10.1093/jxb/erj181.

[40] B. Song, G.L. Wang, M.Q. Tan, J.L. Yuan, A europium(III) complex as an efficient singlet oxygen luminescence probe, J. Am. Chem. Soc. 128 (41) (2006) 13442–13450, https://doi.org/10.1021/ja062990f.

[41] M.Q. Tan, B. Song, G.L. Wang, J.L. Yuan, A new terbium(III) chelate as an efficient singlet oxygen fluorescence probe, Free Radical Biol. Med. 40 (9) (2006) 1644–1653, https://doi.org/10.1016/j.freeradbiomed.2005.12.030.

[42] Y.J. Liu, K.Z. Wang, Visible-Light-Excited Singlet-Oxygen Luminescence Probe Based on Re(CO)3Cl(aeip), Eur. J. Inorg. Chem. 33 (2008) 5214–5219, https://doi.org/10.1002/ejic.200800699.

[43] D.B. Zhu, D. Xing, Y.D. Wei, X. Li, B. Gao, Evaluation of the degree of medical radiation damage with a highly sensitive chemiluminescence method, Luminescence 19 (5) (2004) 278–282, https://doi.org/10.1002/bio.782.

[44] A.M. Falick, B.H. Mahan, R.J. Myers, Paramagnetic resonance Spectrum of the 1Δg oxygen molecule, J. Chem. Phys. 42 (1965) 1837–1838, https://doi.org/10.1063/1.1696199.

[45] R. Vankayala, Ch.-L. Kuo, A. Sagadevan, P.-H. Chen, Ch.-S. Chiang, K.-Ch. Hwang, Morphology dependent photosensitization and formation of singlet oxygen (1Δg) by gold and silver nanoparticles and its application in cancer treatment, J. Mater. Chem. B Mater. Biol. Med. 1 (35) (2013) 4379–4387 https://10.1039/C3TB20806K.

[46] M. Lismont, M. Dreesem, B. Heinrichs, C.A. Paez, Protoporphyrin IX-Functionalized AgSiO2 core–shell nanoparticles: plasmonic enhancement of fluorescence and singlet oxygen production, Photochem. Photobiol. 92 (2) (2016) 247–256, https://doi.org/10.1111/php.12557.

[47] L. Vattuone, M. Rocca, C. Boragno, U. Valbusa, Initial sticking coefficient of O2 on Ag(110), J. Chem. Phys. 101 (1) (1994) 713–725, https://doi.org/10.1063/1.468127.

[48] G. Binsch, E. Heilbronner, R. Jankow, D. Schmidt, On the fluorescence anomaly of azulene, Chem. Phys. Lett. 1 (4) (1967) 135–138, https://doi.org/10.1016/0009-2614(67)85008-5.

[49] R. Vankayala, Y.-K. Huang, P. Kalluru, Ch-Sh. Chiang, K.Ch. Hwang, First Demonstration of Gold Nanorods-Mediated Photodynamic Therapeutic Destruction of Tumors via Near Infra-Red Light Activation, Small 10 (8) (2014) 1612–1622, https://doi.org/10.1002/smll.201302719.

[50] T. Zhao, X. Shen, L. Li, Z. Guan, N. Gao, P. Yuan, S.Q. Yao, Q.-H. Xu, G.Q. Xu, Gold nanorods as dual photo-sensitizing and imaging agents for two-photon

photodynamic therapy, Nanoscale 4 (24) (2012) 7712–7719 https://10.1039/C2NR32196C.
[51] P. Vijayaraghavan, C.-H. Liu, R. Vankayala, C.-S. Chiang, K.C. Hwang, Designing multi-branched gold nanoechinus for NIR light activated dual modal photodynamic and photothermal therapy in the second biological window, Adv. Mater. 26 (39) (2014) 6689–6695, https://doi.org/10.1002/adma.201400703.
[52] G. Pasparakis, Light-induced generation of singlet oxygen by naked gold nanoparticles and its implications to cancer cell phototherapy, Small 9 (24) (2013) 4130–4134, https://doi.org/10.1002/smll.201301365.
[53] J. Ly, X. Zhang, N. Li, B. Wang, H. Sailing, Absorption-dependent generation of singlet oxygen from gold bipyramids excited under low power density, RSC Adv. 5 (100) (2015) 81897–81904, https://doi.org/10.1039/C5RA15362J.
[54] C. Jiang, T. Zhao, P. Yuan, N. Gao, Y. Pan, Z. Guan, N. Zhou, Q.-H. Xu, Two-photon induced photoluminescence and singlet oxygen generation from aggregated gold nanoparticles, ACS Appl. Mater. Interfaces 5 (11) (2013) 4972–4977, https://doi.org/10.1021/am4007403.
[55] R. Vankayala, Ch.-Ch. Lin, P. Kalluru, Ch.-Sh. Chiang, K.Ch. Hwang, Gold nanoshells-mediated bimodal photodynamic and photothermal cancer treatment using ultra-low doses of near infra-red light, Biomaterials 35 (21) (2014) 5527–5538, https://doi.org/10.1016/j.biomaterials.2014.03.065.
[56] A.M. Schwartzberg, T.Y. Olson, Ch.E. Talley, J.Z. Zhang, Synthesis, characterization, and tunable optical properties of hollow gold nanospheres, J. Phys. Chem. B 110 (4) (2006) 19935–19944, https://doi.org/10.1021/jp062136a.
[57] M. Yu, F. Guo, J. Wang, F. Tan, N. Li, Photosensitizer-loaded pH-Responsive hollow gold nanospheres for single light-induced Photothermal/Photodynamic therapy, ACS Appl. Mater. Interfaces 7 (32) (2015) 17592–17597, https://doi.org/10.1021/acsami.5b05763.
[58] H. Kawasaki, S. Kumar, G. Li, Ch. Zheng, D.R. Kauffman, J. Yoshimoto, Y. Iwasaki, R. Jin, Generation of singlet oxygen by photoexcited Au25(SR)18 clusters, Chem. Mater. 26 (9) (2014) 2777–2788, https://doi.org/10.1021/cm500260z.
[59] A.M. Fales, H. Yuan, T. Vo-Dinh, Silica-coated gold nanostars for combined surface-enhanced raman scattering (SERS) detection and singlet-oxygen generation: a potential nanoplatform for theranostics, Langmuir 27 (19) (2011) 12186–12190, https://doi.org/10.1021/la202602q.
[60] M.K. Khaing Oo, X. Yang, H. Du, H. Wang, 5-aminolevulinic acid-conjugated gold nanoparticles for photodynamic therapy of cancer, Nanomedicine 3 (6) (2008) 777–786, https://doi.org/10.2217/17435889.3.6.777.
[61] S.V. Yazdi, M. Darroudi, A. Imanparast, F. Hatominia, A. Sazgarnia, Effect of silver nanoparticles on improving the efficacy of 5-Aminolevulinic acid-induced photodynamic therapy, Iran, J. Med. Phys. 15 (2018) 308–314, https://doi.org/10.22038/ijmp.2017.27921.1301.
[62] J. Zeng, W. Yang, D. Shi, X. Li, H. Zhang, M. Chen, Porphyrin derivative conjugated with gold nanoparticles for dual-modality photodynamic and photothermal therapies in vitro, ACS Biomater. Sci. Eng. 4 (3) (2018) 963–972, https://doi.org/10.1021/acsbiomaterials.7b00886.
[63] Y. Yang, Y. Hu, H. Du, L. Ren, H. Wang, Colloidal plasmonic gold nanoparticles and gold nanorings: shape-dependent generation of singlet oxygen and their performance in enhanced photodynamic cancer therapy, Int. J. Nanomedicine 5 (13) (2018) 2065–2078, https://doi.org/10.2147/IJN.S156347.
[64] M.E. Wieder, D.C. Hone, M.J. Cook, M.M. Handsley, J. Gavrilovic, D.A. Russell, Intracellular photodynamic therapy with photosensitizer-nanoparticle conjugates: cancer therapy using a 'Trojan horse', Photochem. Photobiol. Sci. 5 (8) (2006) 727–734, https://doi.org/10.1039/B602830F.
[65] P. Garcia Calavia, I. Chambrier, M.J. Cook, A.H. Haires, R.A. Field, D.A. Russell, Targeted photodynamic therapy of breast cancer cells using lactose-phthalocyanine functionalized gold nanoparticles, J. Colloid Interface Sci. 15 (512) (2018) 249–259, https://doi.org/10.1016/j.jcis.2017.10.030.
[66] L. Vieria, M.L. Castilho, I. Ferreira, J. Ferreira-Strixino, K.C. Hewitt, L. Raniero, Synthesis and characterization of gold nanostructured Chorin e6 for Photodynamic Therapy, Photodiagnosis Photodyn. Ther. 18 (2017) 6–11, https://doi.org/10.1016/j.pdpdt.2016.12.012.
[67] X. Ke, D. Wang, C. Chen, Co-enhancement of fluorescence and singlet oxygen generation by silica-coated gold nanorods core-shell nanoparticle, Nanoscale Res. Lett. 9 (2014) 666–674, https://doi.org/10.1186/1556-276X-9-666.
[68] Z. Shi, W. Ren, A. Gong, X. Zhao, Y. Zou, E.M. Brown, X. Chen, A. Wu, Stability enhanced polyelectrolyte-coated gold nanorod-photosensitizer complexes for high/low power density photodynamic therapy, Biomaterials 35 (25) (2014) 7058–7067, https://doi.org/10.1016/j.biomaterials.2014.04.105.
[69] J. Baier, T. Maisch, M. Maier, E. Engel, M. Landthaler, W. Bäumler, Singlet oxygen generation by UVA light exposure of endogenous photosensitizers, Biophys. J. 91 (4) (2006) 1452–1459, https://doi.org/10.1529/biophysj.106.082388.
[70] L.S.A. de Melo, A.S.L. Gomes, S. Saska, K. Nigoghossian, Y. Messaddeq, S.J.L. Ribeiro, R.E. de Araujo, Singlet oxygen generation enhanced by silver-pectin, Nanoparticles J. Fluoresc. 22 (6) (2012) 1633–1638, https://doi.org/10.1007/s10895-012-1107-4.
[71] M.B.R. Aiello, D. Castrogiovanni, J. Parisi, J.C. Azcarate, Photodynamic Therapy in HeLa Cells Incubated with Riboflavin and Pectin-coated Silver Nanoparticles, Photochem. Photobiol. 94 (6) (2018) 1159–1161, https://doi.org/10.1111/php.12974.
[72] B. Khlebtsov, E. Panfilova, V. Khanadeev, O. Bibikova, G. Terentyuk, A. Ivanov, V. Rumyantseva, I. Shilov, A. Ryabova, V. Loshchenov, N.G. Khlebtsov, nanocomposites containing silica-coated gold–silver nanocages and Yb–2,4-Dimethoxyhematoporphyrin: multifunctional capability of IR-Luminescence detection, photosensitization, and photothermolysis, ACS Nano 5 (9) (2011) 7077–7089, https://doi.org/10.1021/nn2017974.
[73] T. Nagy-Simon, M. Potara, A.M. Cracium, E. Licarete, S. Astilean, IR780-dye loaded gold nanoparticles as new near infrared activatable nanotheranostic agents for simultaneous photodynamic and photothermal therapy and intracellular tracking by surface enhanced resonant Raman scattering imaging, J. Colloid Interface Sci. 517 (1) (2018) 239–250, https://doi.org/10.1016/j.jcis.2018.02.007.
[74] A. Imanparasta, M. Bakhshizadeh, R. Salek, A. Sazgarnia, Pegylated hollow gold-mitoxantrone nanoparticles combining photodynamic therapy and chemotherapy of cancer cells, Photodiagn. Photodyn. Ther. 23 (2018) 295–305, https://doi.org/10.1016/j.pdpdt.2018.07.011.
[75] P. Kalluru, R. Vankayala, C.-S. Chiang, K.C. Hwang, Photosensitization of singlet oxygen and in vivo photodynamic therapeutic effects mediated by PEGylated W18O49 nanowires, Angew. Chem. 125 (47) (2013) 12558–12562, https://doi.org/10.1002/ange.201307358.
[76] J. Ge, M. Lan, B. Zhou, W. Liu, L. Guo, H. Wang, Q. Jia, G. Niu, X. Huang, H. Zhou, X. Meng, P. Wang, C.S. Lee, W. Zhang, X. Han, A graphene quantum dot photodynamic therapy agent with high singlet oxygen generation, Nat. Commun. 5 (2014) 4596–4904, https://doi.org/10.1038/ncomms5596.
[77] L. Shi, B. Hernandez, M. Selke, Singlet oxygen generation from water-soluble quantum dot − Organic dye nanocomposites, J. Am. Chem. Soc. 128 (19) (2006) 6278–6279, https://doi.org/10.1021/ja057959c.
[78] S. Xu, J. Shen, S. Chen, M. Zhang, T. Shen, Active oxygen species (1O2, O2· −) generation in the system of TiO2 colloid sensitized by hypocrellin B, J. Photochem. Photobiol. B, Biol. 67 (1) (2002) 64–70, https://doi.org/10.1016/S1011-1344(02)00263-4.
[79] A. Lipovsky, Z. Tzitrinovich, H. Friedmann, G. Applerot, A. Gedanken, R. Lubart, EPR study of visible light-induced ROS generation by nanoparticles of ZnO, J. Phys. Chem. C 113 (36) (2009) 15997–16001, https://doi.org/10.1021/jp904864g.
[80] L. Li, J.-F. Zhao, N. Won, H. Jin, S. Kim, J.-Y. Chen, Quantum dot-aluminum phthalocyanine conjugates perform photodynamic reactions to kill cancer cells via fluorescence resonance energy transfer, Nanoscale Res. Lett. 7 (2012) 386–394, https://doi.org/10.1186/1556-276X-7-386.
[81] J.M. Tsay, M. Trzoss, L. Shi, X. Kong, M. Selke, M.E. Jung, S. Weiss, Singlet oxygen production by peptide-coated quantum dot − Photosensitizer conjugates, J. Am. Chem. Soc. 129 (21) (2007) 6865–6871, https://doi.org/10.1021/ja070713i.
[82] J. Sun, Q. Xin, Y. Yang, H. Shah, H. Lao, Y. Qi, J.R. Gong, J. Li, Nitrogen-doped graphene quantum dots coupled with photosensitizers for one-/two-photon activated photodynamic therapy based on a FRET mechanism, Chem. Commun. (Camb.) 54 (7) (2018) 715–718, https://doi.org/10.1039/C7CC08820E.
[83] N. Nwahara, J. Britton, T.H. Nyokong, Improving singlet oxygen generating abilities of phthalocyanines: aluminum tetrasulfonated phthalocyanine in the presence of graphene quantum dots and folic acid, Coord. Chem. Rev. 70 (9) (2017) 1601–1616, https://doi.org/10.1080/00958972.2017.1313975.
[84] J.M. Hsieh, M.-L. Ho, P.-W. Wu, P.-T. Chou, T.T. Tsai, Y. Chi, Iridium-complex modified CdSe/ZnS quantum dots; a conceptual design for bifunctionality toward imaging and photosensitization, Chem. Commun. (Camb.) 0 (6) (2006) 615–617, https://doi.org/10.1039/B517368J.
[85] Y. Zhang, G. Hong, Y. Zhang, G. Chen, F. Li, H. Dai, Q. Wang, Ag2S quantum dot: a bright and biocompatible fluorescent nanoprobe in the second near-infrared window, ACS Nano 6 (5) (2012) 3695–3702, https://doi.org/10.1021/nn301218z.
[86] L.M. Rossi, P.R. Silva, L.L.R. Vono, A.U. Fernandes, D.B. Tada, M.S. Baptista, Protoporphyrin IX nanoparticle carrier: preparation, optical properties, and singlet oxygen generation, Langmuir 24 (21) (2008) 12534–12538, https://doi.org/10.1021/la800840k.
[87] F. Yan, R. Kopelman, The Embedding of Meta-tetra(Hydroxyphenyl)-Chlorin into Silica Nanoparticle Platforms for Photodynamic Therapy and Their Singlet Oxygen Production and pH-dependent Optical Properties, Photochem. Photobiol. 78 (6) (2003) 587–591, https://doi.org/10.1562/0031-8655(2003)0780587TEOMIS2.0.CO2.
[88] X. He, X. Wu, K. Wang, B. Shi, L. Hai, Methylene blue-encapsulated phosphonate-terminated silica nanoparticles for simultaneous in vivo imaging and photodynamic therapy, Biomaterials. 30 (29) (2009) 5601–5609, https://doi.org/10.1016/j.biomaterials.2009.06.030.
[89] B. Zhao, J.J. Yin, P.J. Bilski, C.F. Chignell, J.E. Roberts, Y. He, Enhanced photodynamic efficacy towards melanoma cells by encapsulation of Pc4 in silica nanoparticles, Toxicol. Appl. Pharmacol. 241 (2) (2009) 163–172, https://doi.org/10.1016/j.taap.2009.08.010.
[90] T. Wang, L. Zhang, Z. Su, C. Wang, Y. Liao, Q. Fu, Multifunctional hollow mesoporous silica nanocages for Cancer cell detection and the combined chemotherapy and photodynamic therapy, ACS Appl. Mater. Interfaces 3 (7) (2011) 2479–2486, https://doi.org/10.1021/am200364e.
[91] D.B. Tada, L.L. Vono, E.L. Duarte, R. Itri, P.K. Kiyohara, M.S. Baptista, L.M. Rossi, Methylene blue-containing silica-coated magnetic particles: a potential magnetic carrier for photodynamic therapy, Langmuir 23 (15) (2007) 8194–8199, https://doi.org/10.1021/la700883y.
[92] K.A. Fudimura, A.B. Seabra, M.C. Santos, P.S. Haddad, Synthesis and characterization of methylene blue-containing silica-coated magnetic nanoparticles for photodynamic therapy, J. Nanosci. Nanotechnol. 17 (1) (2017) 133–142, https://doi.org/10.1166/jnn.2017.12715.
[93] S. Bharathiraja, M.S. Moorthy, P. Manivasagan, H. Seo, K.D. Lee, J. Oh, Chlorin e6 conjugated silica nanoparticles for targeted and effective photodynamic therapy, Photodiagnosis Photodyn. Ther. 19 (2017) 212–220, https://doi.org/10.1016/j.pdpdt.2017.06.001.
[94] Z. Youssef, V. Jouan-Hureaux, L. Colombeau, P. Arnoux, A. Moussaron, F. Baros, J. Toufaily, T. Hamieh, T. Roques-Carmes, C. Frochot, Titania and silica

nanoparticles coupled to Chlorin e6 for anti-cancer photodynamic therapy, Photodiagnosis Photodyn, Ther. 22 (2018) 115–126, https://doi.org/10.1016/j.pdpdt.2018.03.005.
[95] B. Zhou, B. Shi, D. Jin, X. Liu, Controlling upconversion nanocrystals for emerging applications, Nat. Nanotechnol. 10 (11) (2015) 924–936, https://doi.org/10.1038/nnano.2015.251.
[96] M. Mahboub, Z. Huang, M.L. Tang, Efficient infrared-to-Visible upconversion with subsolar irradiance, Nano Lett. 16 (11) (2016) 7169–7175, https://doi.org/10.1021/acs.nanolett.6b03503.
[97] P. Zhang, W. Steelant, M. Kumar, M. Scholfield, Versatile photosensitizers for photodynamic therapy at infrared excitation, J. Am. Chem. Soc. 129 (15) (2007) 4526–4527, https://doi.org/10.1021/ja0700707.
[98] F. Lin, A.W. Girotti, The pecking order of free radicals and antioxidants: lipid peroxidation, α-Tocopherol, and ascorbate, Arch. Biochem. Biophys. 300 (2) (1993) 714–723, https://doi.org/10.1006/abbi.1993.1074.
[99] F. Chen, S. Zhang, W. Bu, Y. Chen, Q. Xiao, J. Liu, H. Xing, L. Zhou, W. Peng, J. Shi., A Uniform Sub-50 nm-Sized Magnetic/Upconversion Fluorescent Bimodal Imaging Agent Capable of Generating Singlet Oxygen by Using a 980 nm Laser, Chemistry. 18 (23) (2012) 7082–7090, https://doi.org/10.1002/chem.201103611.
[100] F. Lu, L. Yang, Y. Ding, J.J. Zhu, Highly Emissive Nd3 + -Sensitized Multilayered Upconversion Nanoparticles for Efficient 795 nm Operated Photodynamic Therapy, Adv. Funct. Mater. 26 (26) (2016) 4778–4785, https://doi.org/10.1002/adfm.201600464.
[101] T. Sabri, P.D. Pawelek, J.A. Capabianco, Dual activity of rose bengal functionalized to albumin-coated lanthanide-doped upconverting nanoparticles: targeting and photodynamic therapy, ACS Appl. Mater. Interfaces 10 (32) (2018) 26947–26953, https://doi.org/10.1021/acsami.8b08919.
[102] F. Xu, L. Ding, W. Tao, X. Yang, H. Qian, R. Yao, Mesoporous-silica-coated upconversion nanoparticles loaded with vitamin B12 for near-infrared-light mediated photodynamic therapy, Mater. Lett. 167 (2016) 205–208, https://doi.org/10.1016/j.matlet.2015.12.105.
[103] M.R. Hamblin, Upconversion in photodynamic therapy: plumbing the depths, Dalton Trans. 47 (26) (2018) 8571–8580, https://doi.org/10.1039/C8DT00087E.
[104] H. Guo, H. Qian, N.M. Idris, Y. Zhang, Singlet oxygen-induced apoptosis of cancer cells using upconversion fluorescent nanoparticles as a carrier of photosensitizer, Nanomedicine 6 (3) (2010) 486–495, https://doi.org/10.1016/j.nano.2009.11.004.
[105] L. Xia, X. Kong, X. Liu, L. Tua, Y. Zhang, Y. Chang, Liu K, D. Shen, H. Zhao, H. Zhang, An upconversion nanoparticle – Zinc phthalocyanine based nanophotosensitizer for photodynamic therapy, Biomaterials 35 (13) (2014) 4146–4156, https://doi.org/10.1016/j.biomaterials.2014.01.068.
[106] C. Wang, H. Tao, L. Cheng, Z. Liu, Near-infrared light induced in vivo photodynamic therapy of cancer based on upconversion nanoparticles, Biomaterials 32 (26) (2011) 6145–6154, https://doi.org/10.1016/j.biomaterials.2011.05.007.
[107] Q. Yu, E.M. Rodriguez, R. Naccache, P. Forgione, G. Lamoureux, F. Sanz-Rodriguez, D. Scheglmann, J.A. Capobianco, Chemical modification of temoporfin – a second generation photosensitizer activated using upconverting nanoparticles for singlet oxygen generation, Chem. Commun. (Camb.) 50 (81) (2014) 12150–12153, https://doi.org/10.1039/C4CC05867D.
[108] L. Xia, X. Kong, X. Liu, L. Tu, Y. Zhang, Y. Chang, K. Liu, D. Shen, H. Zhao, H. Zhang, An upconversion nanoparticle–Zinc phthalocyanine based nanophotosensitizer for photodynamic therapy, Biomaterials 35 (14) (2014) 4146–4156, https://doi.org/10.1016/j.biomaterials.2014.01.068.
[109] H.S. Qian, H.C. Guo, P.C. Ho, R. Mahendran, Y. Zhang, Mesoporous-Silica-Coated Up-Conversion Fluorescent Nanoparticles for Photodynamic Therapy, Small 5 (20) (2009) 2285–2290, https://doi.org/10.1002/smll.200900692.
[110] Z. Zhao, Y. Han, C. Lin, D. Hu, F. Wang, X. Chen, Z. Chen, N. Zheng, Multifunctional core-shell upconverting nanoparticles for imaging and photodynamic therapy of liver cancer cells, Chem. Asian J. 7 (4) (2012) 830–837, https://doi.org/10.1002/asia.201100879.
[111] Q.Q. Dou, Ch.P. Teng, E. Ye, X.J. Loh, Effective near-infrared photodynamic therapy assisted by upconversion nanoparticles conjugated with photosensitizers, Int. J. Nanomedicine 10 (2015) 419–432, https://doi.org/10.2147/IJN.S74891.
[112] Xu H, P. Yang, M. Sun, H. Bi, B. Liu, D. Yang, S. Gai, F. He, J. Lin, Highly emissive dye-sensitized upconversion nanostructure for dual-photosensitizer photodynamic therapy and bioimaging, ACS Nano 11 (4) (2017) 4133–4144, https://doi.org/10.1021/acsnano.7b00944.
[113] S.S. Lucky, N. Muhammad Idris, Z. Li, K. Huang, K.C. Soo, Y. Zhang, Titania coated upconversion nanoparticles for near-infrared light triggered photodynamic therapy, ACS Nano 9 (1) (2015) 191–205, https://doi.org/10.1021/nn503450t.
[114] D. Zhang, L. Wen, R. Huang, H. Wang, X. Hu, D. Xing, Mitochondrial specific photodynamic therapy by rare-earth nanoparticles mediated near-infrared graphene quantum dots, Biomaterials 153 (2018) 14–26, https://doi.org/10.1016/j.biomaterials.2017.10.034.
[115] S.Y. Choi, S.H. Baek, S.J. Chang, Y. Song, R. Rafique, K.T. Lee, T.J. Park, Synthesis of upconversion nanoparticles conjugated with graphene oxide quantum dots and their use against cancer cell imaging and photodynamic therapy, Biosens. Bioelectron. 93 (2017) 267–273, https://doi.org/10.1016/j.bios.2016.08.094.
[116] X. Wang, J. Xu, D. Yana, Ch. Sun, Q. Sun, F. He, S. Gai, Ch. Zhong, Ch. Li, P. Yang, Fe3O4@MIL-100(Fe)-UCNPs heterojunction photosensitizer: rational design and application in near infrared light mediated hypoxic tumor therapy, Chem. Eng. J. 354 (2018) 1141–1152, https://doi.org/10.1016/j.cej.2018.08.070.
[117] D. Wang, L. Zhu, Y. Pu, J.X. Wang, J.F. Chen, L. Dai, Transferrin-coated magnetic upconversion nanoparticles for efficient photodynamic therapy with near-infrared irradiation and luminescence bioimaging, Nanoscale 9 (31) (2017) 11214–11221, https://doi.org/10.1039/C7NR03019C.
[118] J. Liu, L. Huang, X. Tian, X. Chen, Y. Shao, F. Xie, D. Chen, L. Li, Magnetic and fluorescent Gd2O3:Yb3 + /Ln3 + nanoparticles for simultaneous upconversion luminescence/MR dual modal imaging and NIR-induced photodynamic therapy, Int. J. Nanomedicine 12 (2016) 1–14, https://doi.org/10.2147/IJN.S118938.
[119] X. Zou, M. Yao, L. Ma, M. Hossu, X. Han, P. Juzenas, W. Chen, X-ray-induced nanoparticle-based photodynamic therapy of cancer, Nanomedicine 9 (15) (2014) 2339–2351, https://doi.org/10.2217/nnm.13.198.
[120] A.-L. Bulin, C. Truillet, R. Chouikrat, F. Lux, C. Frochot, D. Amans, G. Ledoux, O. Tillement, P. Perriat, M. Barberi-Heyob, C. Dujardin, X-ray-induced singlet oxygen activation with nanoscintillator-coupled porphyrins, J. Phys. Chem. C 117 (41) (2013) 21583–21589, https://doi.org/10.1021/jp4077189.
[121] Y. Liu, W. Chen, S. Wang, A.G. Joly, Investigation of water-soluble x-ray luminescence nanoparticles for photodynamic activation, Appl. Phys. Lett. 92 (4) (2008) 043901-1–043901-3, https://doi.org/10.1063/1.2835701.
[122] Y. Tang, J. Hu, A.H. Elmenoufy, X. Yang, Highly efficient FRET system capable of deep photodynamic therapy established on X-ray excited mesoporous LaF3:Tb scintillating nanoparticles, ACS Appl. Mater. Interfaces 7 (22) (2015) 12261–12269, https://doi.org/10.1021/acsami.5b03067.
[123] L. Ma, X. Zou, B. Bui, W. Chen, K. Hyun Song, T. Solberg, X-ray excited ZnS:Cu,Co afterglow nanoparticles for photodynamic activation, Appl. Phys. Lett. 105 (1) (2014) 013702-1–013702-5, https://doi.org/10.1063/1.4890105.
[124] J. Takahashi, M. Misawa, Analysis of potential radiosensitizing materials for X-Ray-Induced photodynamic therapy, Nanobiotechnology 3 (2) (2007) 116–126, https://doi.org/10.1007/s12030-008-9009-x.
[125] P. Huang, Le. Bao, Ch. Zhang, J. Lin, T. Luo, D. Yang, M. He, Z. Li, G. Gao, B. Gao, S. Fu, D. Cu, Folic acid-conjugated Silica-modified gold nanorods for X-ray/CT imaging-guided dual-mode radiation and photo-thermal therapy, Biomaterials 32 (36) (2011) 9796–9809, https://doi.org/10.1016/j.biomaterials.2011.08.086.